Image Registration and Fusion
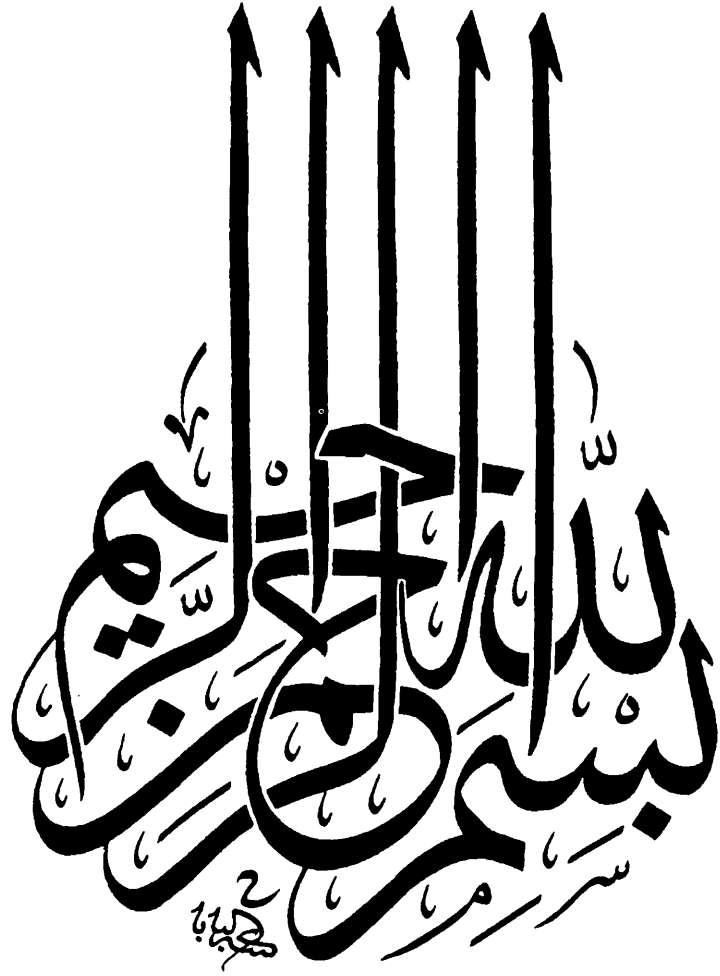
by

Isam H. Habboush

Submitted to the Department of
Nuclear Engineering in Partial Fulfillment of
the Requirements for the
Degree of

MASTER OF SCIENCE

at the

Massachusetts Institute of Technology

May 1995

© 1995 Massachusetts Institute of Technology
All rights reserved

The author hereby grants to MIT permission to reproduce and to
distribute publicly paper and electronic copies of this thesis
document in whole or in part.

Signature of Author ....
Department of Nuclear Engineering
May 12, 1995

Certified by ....
Dr. S.T. Treves
Thesis Supervisor

Certified by ....
Professor David Cory
Thesis Reader

Accepted by ....
/Professor Allan Henry
Departmental Committee on Graduate Studies

بسم الله الرحمن الرحيم

Image Registration and Fusion

by

Isam H. Habboush

ABSTRACT

The aim of image registration is to align corresponding structures of two or more 3-D images geometrically. This is used to accurately correlate functional information derived from SPECT with anatomical information derived from MRI, and to assess changes in serial SPECT studies. A number of registration techniques have been proposed. These methods are based on extracting features from the images and using iterative techniques to minimize an error residual. We review these techniques and observe three common weak points: the lack of control of the operator over registration, the inability to align single studies, and the inability to register ^{201}Tl-SPECTs with other studies. Although these methods are automated, the final decision on the validity of registration is left to the inspection of a trained operator. This thesis examines the possibility and practicality of manual registration. We explore this by developing a manual registration algorithm which provides the user with real time feedback information about the orientation and location of images in 3-D and tools to manipulate these images geometrically. Furthermore, the algorithm provides the user with information about the relative location and orientation of the images. This is done through the use

3

of grid lines, overlapping, and fusion of images in different colors. This manual registration method gives the operator full control of registration, capable of aligning single studies to any orientation, and capable of registering ^{201}Tl-SPECTs to perfusion SPECT or MRI.

The accuracy and consistency of this method is assessed using both phantom and clinical brain studies. The studies used for validation consisted of five SPECTs of a brain phantom with known miss-registrations and an MRI of the same phantom and eight pairs of clinical brain studies. Three individuals were asked to register the SPECTs to each others, the SPECTs to the MRI, and each pair of the clinical studies. Registration of SPECT to SPECT of the brain phantom yielded accuracy of 1.5 pixels (3.6 mm). Registration of SPECTs to MRI of the same phantom yielded consistency of 0.7 pixels (1.7 mm) among the three operators. Registration of the clinical studies yielded consistency of 0.5 pixels (1.2 mm) among the same operators.

Thesis Supervisor: Dr. S.T. Treves
Title: M.D.

4

Acknowledgments

It is beyond my words to express my gratitude to all of these people who helped my during this time. However, I would like to take this opportunity to acknowledge and thank the following people.

Table Of Contents

List of Figures

8

List of Tables

Chapter 1

You see things and you say "Why?"; but I dream
things that never were and I say "Why not?"

— George Bernard Shaw

Introduction

With significant technical advances in three dimensional (3-D) diagnostic imaging (CT, MRI, SPECT, PET) the need to relate physiologic, or metabolic changes to anatomic information has increased. In many cases, interpretation is aided if images depicting regional function are overlaid on structural images in three dimensions. In the past, physicians have relied on their spatial sense to mentally reorient and overlap images from different imaging modalities. This approach, of course, is highly subjective and inconsistent. Objective methods for image alignment and registration are needed.

Image alignment is used in order to reorient an image in 3-D with respect to some standard reference planes. This has to be done consistently and reliably so that, for example, transverse slices of the brain show left vs. right information on the same horizontal plane. Image registration, on the other hand, facilitates comparison of two or more 3-D imaging studies of the same organ or system. This technique is useful to determine functional and anatomical relationships. An example of this is the registration of an ictal

perfusion brain SPECT with the corresponding MRI to determine the location of an ictal foci. Another example is to compare the uptake of a tumor seeking radiopharmaceutical (i.e. ^{201}Tl) with MRI findings in a patient following treatment of brain tumor where differentiation of tumor recurrence from fibrosis or necrosis is unclear. Another application of image registration is to evaluate an organ in two different functional states. For example to compare the distribution of regional cerebral perfusion in an ictal and an interictal brain SPECT.

1.1   Image   Registration

In order to compare 3-D image sets obtained from various imaging modalities it is necessary to convert the images of those imaging modalities to a single dimensional scale (scaling). Once the images are scaled they must be oriented in the same orthogonal planes (registration). Registered 3-D images can be superimposed and displayed to demonstrate functional and anatomical relationships (fusion).

Difficulties encountered in registering functional and anatomic images include physical limitations and imaging target. Physical limitations are associated with the relatively lower spatial resolution and low signal-to-noise ratio of functional (i.e. SPECT) vs. structural imaging modalities (i.e. MRI). Imaging target, on the other hand, is modality dependent. For example, SPECT represents the function of an organ by mapping regional perfusion or metabolism. If part of

the organ is not perfused or is metabolically inactive, it will not be visualized on SPECT. On the other hand, MRI represents the structure of the part of the body that is being imaged and is less dependent on perfusion or metabolic activity. Therefore, it is crucial to identify some common features (or landmarks) on both sets of images that can be used in the registration process.

1.2 Image Registration Techniques

Image registration requires two 3-D images, a reference image and an active image. Once aligned, the reference image is fixed in space while the active image is transformed geometrically until it is registered to the reference image (Figure 1.1). The geometric transform function, or registration transfer, is the transform that achieves best fit of the two images. It is estimated from some similar properties of the two images.
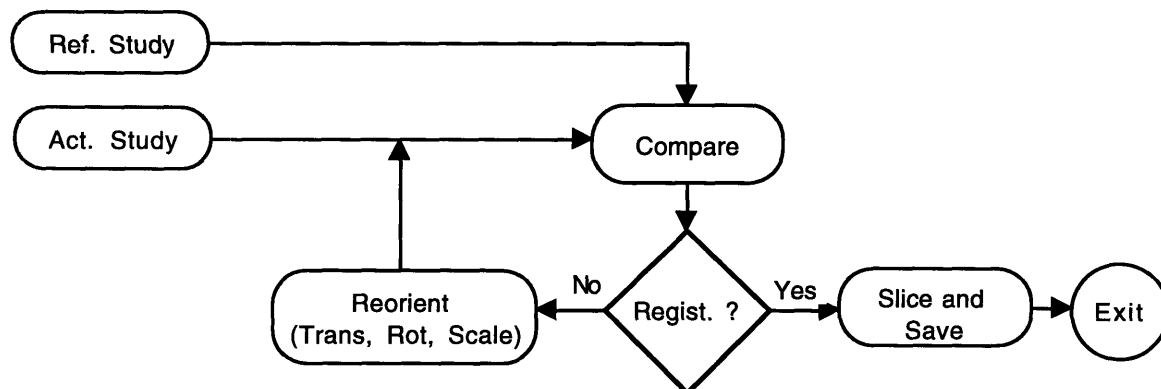
Figure 1.1 Diagram for registration of two studies, active and reference.

Many registration techniques have been proposed. These techniques differ in the type of information they extract from the images and in the way they determine the registration transform. In order to discuss and compare these techniques, it is necessary to compile image registration in a common frame. Image registration in general can be viewed as an operation which consists of three components:

(i)   Extraction of features from images.

(ii)   Calculation of the registration transform.

(iii) Measurement of the quality of fit.

Images are constructed or processed in order to extract particular features or parameters such as edges or moments. These features are then used in the registration algorithm. The main objective of the registration algorithm is to determine the registration transform of the reference and active images. The registration transform is either calculated analytically or estimated iteratively depending on the registration technique.

The fundamental requirement of any registration approach is the ability to determine accurately and reliably the degree and quality of fit between images and thus the validity of the registration transform. This can be accomplished in a number of ways, which are commonly referred to as similarity measures. Examples of these similarity measures include correlation function (CF), correlation coefficient (CC), sum of absolute value difference (SAVD), root mean square error (RMS), and stochastic sign change (SSC). (Venot 1984, Venot 1986, Svedlow 1978)

Image registration methods can be classified based on the type of parameters or properties derived from the images, the method by which the registration transform is estimated, and the similarity measure that is used. In this work, we use the first criteria for classification. We define four broad classes of registration methods: registration using external markers, analytical registration, surface registration, and volume registration. These methods vary in their stability depending on the amount of information incorporated in the registration process. For example, registration algorithms that depend on surface information only tend to be sensitive to errors in edge definition. On the other hand, registration algorithms that incorporate information from internal structures as well as external surfaces tend to be more stable. (Chen 1993, Corria 1990, Pelizzari 1989, Barrow 1977, Alpert 1990, Woods 1992)

1.3 About this Thesis

Although the registration methods of the previous section are based on quantitative mathematical models, often, these models are inaccurate or insufficient and the final decision on the validity and accuracy of registration is left to a trained operator. We test the hypothesis that a trained operator can register images manually with satisfactory accuracy with out the need for elaborate mathematical modeling or optimization techniques. Thus, the aim of this thesis is to explore the possibility and practicality of using a manual method for image registration. For a manual method to be successful, it

should give the operator tools for the manipulation of images geometrically and optimal real time feedback about the quality of registration.

We present a manual registration algorithm which we call ALIGN. It divides the 3-D registration problem into three 2-D sub problems, each of which is easy to register. Furthermore, it provides the operator with tools to assess the accuracy of registration through the use of grid lines, and overlapping and fusion of images in different colors. Due to the large amount of data involved in 3-D image registration, ALIGN dynamically extracts only the required slices necessary to show the most recent orientation and location of the images in 3-D. This way, ALIGN gives real time feedback of registration with out the necessary overhead cost of transforming the full data set after each iteration. The actual transformation of the full data set is done at the end of the registration process.

An overview of imaging principles and methods for both SPECT and MRI is presented in the following chapter. Different registration methods are briefly reviewed in chapter 3. In Chapter 4, we shall introduce our manual registration algorithm, ALIGN. It will be shown that ALIGN provides intuitive and robust image manipulation tools which make it ideal for the registration of noisy images like SPECT. The accuracy of the method will be assessed using both phantom and clinical studies in chapter 5. Finally, we discuss the practicality of ALIGN and we present some clinical examples of registered patient images.

Chapter 2

People have now-a-days got a strange opinion that everything should be taught by lectures. Now, I cannot see that lectures can do so much good as reading the books from which the lectures are taken.

— Dr. Johnson (1766)

Imaging Principles

Imaging science is concerned with evaluating the structure of an object by the way it modifies certain properties of a probe, the field of radiation that is used to interrogate the object. In practice, this involves finding methods to invert a class of integral equations. This process is usually called solving the inverse problem in which we measure the changes of our probe and we want to deduce the shape or the structure of the object that caused these changes. Full knowledge of the properties of the probe and the way it interacts with the medium is essential.

The imaging process is normally formulated using linear system theory. In this formalism, the solution to the inverse problem is derived in a closed form using the properties of linear systems. Unfortunately, the interaction mechanisms of radiation with mediums are not linear in general. In such cases, an analytical solution to the inverse problem is very difficult to obtain. Alternatively interative techniques are used to find the most

plausible solution for a given set of initial and boundary conditions. A treatment of such a topic is beyond the scope of this work. Interested readers should consult the references.

This chapter discusses some of the aspects involved in acquiring and reconstructing images in single photon emission computed tomography (SPECT) and magnetic resonance imaging (MRI). The discussion will be general in nature and will only concentrate on the aspects that are related to understanding the necessity and usefulness of image registration. The references contain a list of articles and books that cover these modalities in greater details.

2.2 Nuclear medicine imaging and SPECT

Nuclear medicine imaging provides *in vivo* maps of the distribution of a gamma emitting radionuclide like technetium-99m (^{99m}Tc). The radionuclide is used to label a pharmaceutical which is injected in the patient and based on its chemical properties localizes in special sites or organs. Therefore emission tomography is used indirectly to detect the location of the specific pharmaceutical. Different pharmaceuticals have been developed which target physiologic functions or pathologic processes. For example, lesions and functional states of organs can be evaluated effectively using nuclear medicine techniques. We are interested here in tomographic imaging of the brain in which 2D projections at different angles are used to reconstruct a 3D map of the distribution of the radiopharmaceutical. In particular, we will discuss Single Photon Emission Computed

Tomography (SPECT). First, we will introduce some of the radiopharmaceuticals that are used in brain SPECT and their detection using the Anger camera. Then, tomographic imaging is presented briefly.

2.2.1 Radiopharmaceuticals

Many radionuclides have been used both in vitro and in vivo to trace various biologic processes. Suitable nuclides have γ-ray energies between 60 and 600 keV and have physical properties such that a usable photon flux is available for the diagnostic study without excessive absorbed radiation dose to the patient. In addition, ready availability and low cost are important. The ability to incorporate radionuclides with optimal decay characteristics into appropriate molecules has been the foremost consideration in the development of radiopharmaceuticals. However, many of these radionuclides have been chosen because of their practicality, i.e. no nuclear reactor needed and suitable half life, or low cost (Jaszczak 1988).

The most commonly used radionuclide in nuclear medicine is technetium-99m (^{99m}Tc). Some of its desirable physical characteristics are its 6-hr physical half life and the absence of β radiation which result in low dose to the patient. Also, it emits 140-keV γ radiation which has satisfactory tissue penetration (50% is absorbed in 4.6 cm of tissue), and the energy is low enough to be collimated easily. Two commonly used brain perfusion agents that are labeled with Tc^{99m} are ^{99m}Tc-HMPAO Examethazine (Ceretec, Amersham Co., Arlington Heights, IL) (Figure 2.1a) and ^{99m}Tc-ECD

18

(Neurolite, DuPont Merck, Billerica, MA) (Figure 2.1b). These tracers are trapped intracellularly in the brain according to regional cerebral blood flow. Once taken up, tracer remains fixed, and there is no significant redistribution over several hours (Treves 1995).

Other compounds have been used to image and assess viability of tumors. A notable example is thallium-201 (^{201}Tl) (Figure 2.1c). This compound accumulates in active tumor cells after injection. It remains there for a sufficiently long time to allow imaging.

a)
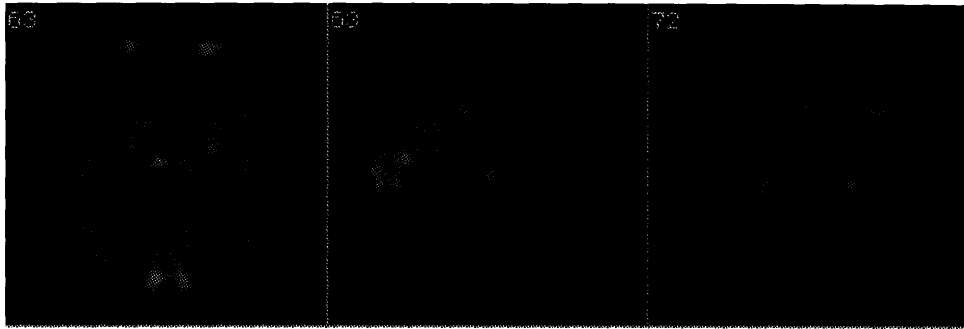
b)
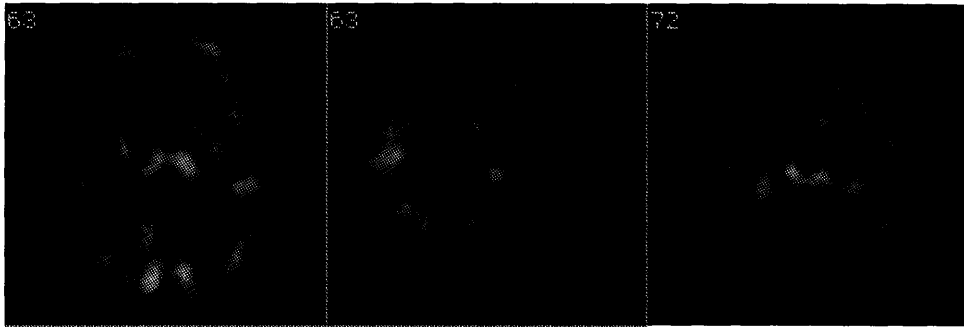
c)
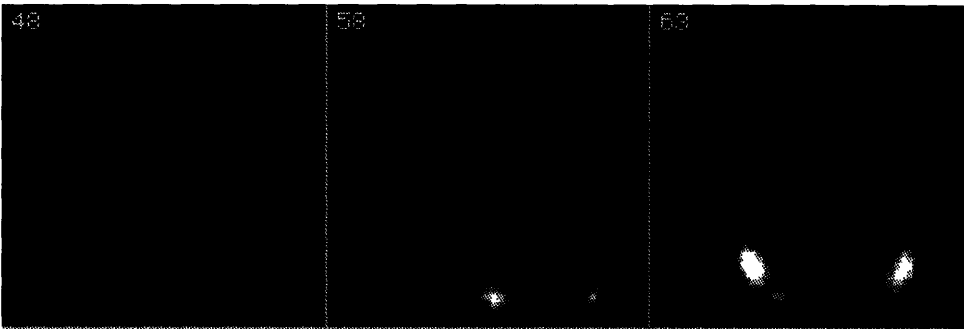
Figure 2.1 Brain SPECT examples. a) ^{99m}Tc-HMPAO. b) ^{99m}Tc-ECD.
c) ^{201}Tl.

2.2.2 The Anger Scintillation Camera

The scintillation camera consists of a single, large diameter NaI(Tl) crystal and an array of photomultiplier tubes (PMT). A lead collimator is used to form an image on the crystal. When a gamma ray interacts with the crystal, its energy is transformed to light. This light is collected by the PMT's. The PMT with the closest proximity to the interaction site of the gamma ray in the crystal will produce the largest output signal, while the more distant tubes will have smaller outputs. By appropriately combining the output signals from all of the tubes, it is possible to compute the centroid of the light distribution, thus determining the coordinates of the interaction site. This principle of 2-D localization was first developed by Anger Camera (Anger 1957). The collimator is made of lead or alloy and is about 2-3 cm. in thickness. It contains small channels that allow gamma rays with appropriate trajectories to reach the crystal. A commonly used collimator contains holes that are parallel to each other and perpendicular to the crystal and is referred to as a parallel hole collimator. The resulting image is a 2-D projection of the 3-D source distribution. Figure 2.2 shows the set up for the Anger scintillation camera.
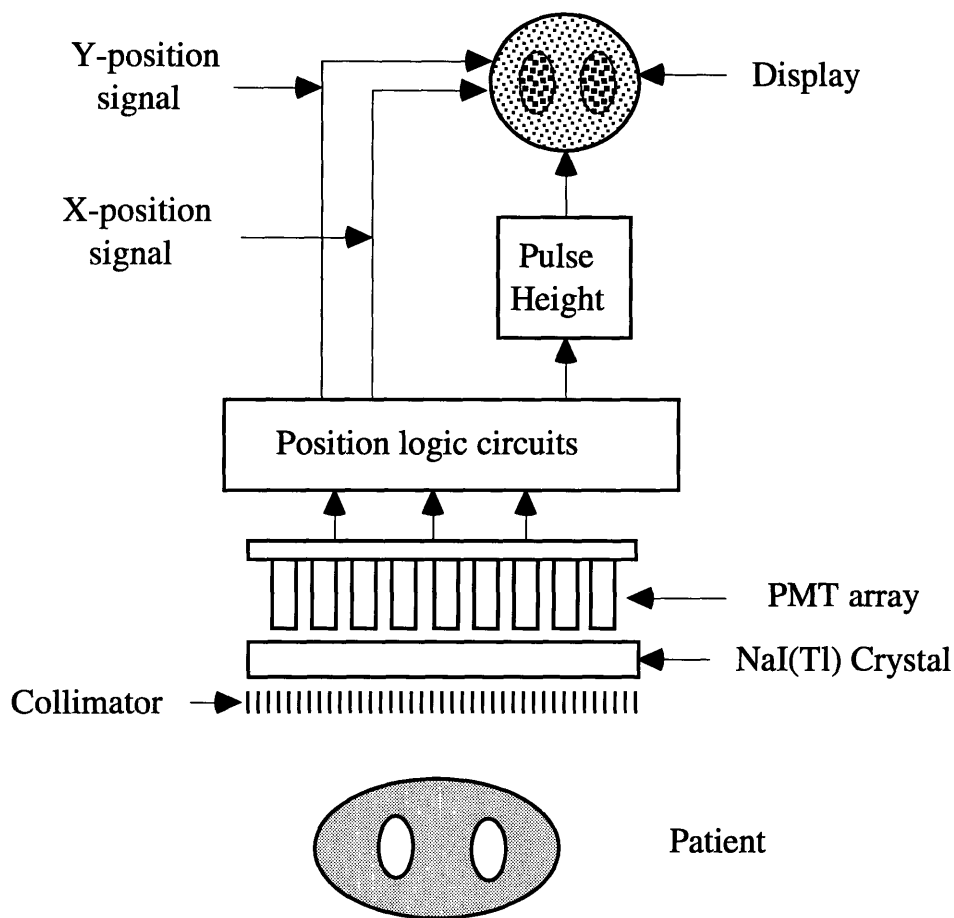
Figure 2.2 Basic principles of the Anger camera.

2.2.3 Tomographic Imaging

Tomographic imaging involves reconstructing a 3-D image from a number of 2-D projections. Usually, 60-120 projections are taken at even intervals around a full circle (360°) around the object. These projections are processed and back-projected radially at the same sampling angles. The reconstructive process described here is called Filtered Back-Projection, which is used in commercial CT and SPECT

scanners.   The development follows that described in the review by Brooks and Di Chiro, (Brooks 1976).

1) Projections Acquisition

An (x,y) coordinate system is used to describe points in the area under investigation (Figure 2.3).   The contribution of each point towards the detected signal is denoted by the distribution function f(x,y) .   A ray projection of this distribution function on a plane at angle ϕ, p(r,ϕ), is denoted by

$$p(r,\phi) = \int_{r,\phi} f(x,y)ds,$$

where ds is the differential path length along a ray.
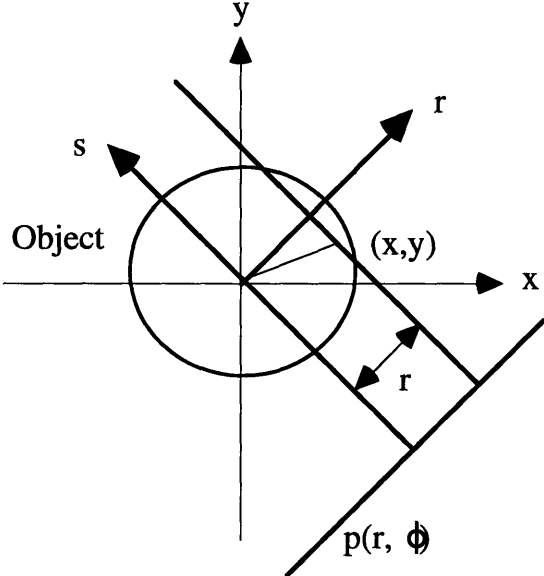
Figure 2.3   Set up and coordinate definition for projections.

2) Simple Back-Projection

23

The ray-projection profiles can be back-projected across a plane on the same angular orientation with which they were acquired, i.e. the magnitude of each projection is applied to all points that make up the ray. The process can be described by

$$\hat{f}(x,y) = \sum_{j=1}^{m} p(x\cos\phi_j + y\sin\phi_j, \phi_j)\Delta\phi$$

where the summation all of the m projections at the specified angles. The hat emphasizes the value is only an approximation of the true density distribution, f(x,y).

Simple back-projection does not produce good results because the values of the projections are applied equally to pixels that contributed to the projections and to pixels with no radioactivities. The resultant image displays discrete areas of high signal which is commonly referred to as a star artifact. As a result, Filtered Back-projection was developed to compensate for some of the short comings of the simple back-projection algorithm. Filtered back-projection will be introduced in the following few sections.

3) Fourier Reconstruction

The density distribution f(x,y) can be represented as a 2-D Fourier integral

$$f(x,y) = \iint_{\infty} F(k_x, k_y)\exp[2\pi i(k_x x + k_y y)]dk_x dk_y$$

24

where k_x and k_y are the wave number in the x and y directions respectively. The Fourier coefficients $F(k_x,k_y)$ are given by the inverse Fourier transform

$$F(k_x,k_y) = \iint_\infty f(x,y)\exp[-2\pi i(k_x x + k_y y)]dxdy$$

By rotating the (x,y) axes to (r,s) axes by the angle

$$\phi = \tan^{-1}\left(\frac{k_y}{k_x}\right)$$

and using the definition

$$k = \sqrt{k_x^2 + k_y^2}$$

the Fourier transform can be written as

$$F(k_x,k_y) = \iint_\infty f(x,y)\exp[-2\pi i k_y r]drds$$

By performing the s-integral we obtain the ray-projection

$$F(k_x,k_y) = \int_\infty p(r,\phi)\exp[-2\pi i k_y r]dr = P(k,\phi)$$

where this equation also defines the Fourier transform for the ray-projection.

Now by writing the equation for the simple back-projection algorithm in integral form

2 5

$$\hat{f}(x,y) = \int p(x\cos\phi + y\sin\phi, \phi)d\phi$$
$$\infty$$

and by replacing $p(x\cos\phi + y\sin\phi, \phi)$ by its Fourier representation

$$p(r,\phi) = \int P(k,\phi)\exp(2\pi ikr)dk$$
$$\infty$$

we get the following important equation

$$\hat{f}(x,y) = \int\limits_{0}^{\pi}\int\limits_{-\infty}^{\infty} \frac{P(k,\phi)}{|k|}\exp[2\pi ik(x\cos\phi + y\sin\phi)]|k|dkd\phi$$

The integrand is multiplied and divided by |k| so that the integral has the form of a 2-D Fourier integral in polar coordinates. By taking the inverse Fourier transform of the above equation we realize the following relation

$$\hat{F}(k_x,k_y) = \frac{P(k,\phi)}{|k|} = \frac{F(k_x,k_y)}{|k|}$$

where

$\hat{F}(k_x,k_y)$ is the Fourier transform of the back-projected image.

$P(k,\phi)$ is the Fourier transform of the projection, and

$F(k_x,k_y)$ is the Fourier transform of the true image.

The above equation shows that the back-projected image is equal to the true image but is scaled by the spatial frequency, k.

4) Filtered Back-projection

The Filtered back-projection algorithm follows the development introduced in the previous section. It consists of the following steps:

26

i) Take the Fourier transform of a projection.

ii) Multiply by |k|, Or equivalently convolve the real projection data by the transform of |k|.

iii) Back-project onto image plane.

iv) Repeat for all projection.

v) Take 2-D inverse Fourier transform to recover image.

5) Limitations

The previous development neglected some very important limitations on pure filtered back-projection reconstruction. For example, attenuation and scatter of photons in the object were not accounted for. Some corrections in association with the filtered back-projection algorithm can be applied to compensate partially for some of the limitations. Also, iterative reconstruction techniques are being developed which may provide more accurate reconstruction. The discussion of these algorithms is beyond the scope of this chapter and interested readers should consult the references (Brooks 1976, Jaszczak 1988).

2.2.4 Conclusion

SPECT gives a 3D map of the distribution of a radionuclide labeled pharmaceutical. Limitations on the quality of SPECT may be the result of some of the following factors:

1) Insufficient counts

Grainy and noisy images is a characteristic of nuclear medicine images in general. The two factors affecting this the most are the

desire to inject the lowest possible amount of activity in the patient, thus decreasing the total dose. The second reason is that the imaging time should be kept as short as practically possible. Lengthy scans in general are inconvenient to the patient and are susceptible to motion.

2) Attenuation and Scatter

Attenuation may result in lower apparent counts in the image than in the actual object. Scatter may result in counts in areas in the image that correspond to regions with no tracer in the object thus giving erroneous tracer distribution. Unfortunately, no suitable solution has been found to correct for these two factors and this remains to be an active area of research.

3) Pharmaceutical distribution

To extract accurate physiologic information requires that the transit of tracer through the body be appropriately modeled. The model used is specific to each radiopharmaceutical, organ, system, and study. Inaccuracies in the model may lead to misinterpretation of the images and thus compromise the quality and usefulness of study.

From the previous discussion, it should be clear that the general quality of SPECT in terms of signal to noise and anatomical information is lower than that of MRI or CT. Although modern equipment have high detection efficiency and better signal processing algorithms, MRI and CT will remain the reference technique for imaging anatomy. Thus, registration of SPECT with an

anatomical based modality, e.g. MRI, is very desirable for the reasons outlined briefly in Chap. 1.

2.3 Magnetic Resonance Imaging (MRI)

2.3.1 Introduction

Magnetic resonance is a phenomenon found in magnetic systems that posses both magnetic moments and angular momentum. The term resonance implies that the scanner is in tune with a natural frequency of the magnetic system. The advantage of the resonance methods is that it enables one to select out of the total magnetic susceptibility, a particular contribution of interest, which may be relatively weak. Resonance also permits the gathering of precise and highly detailed magnetic information of type not obtainable in other ways.

One of the most active applications of nuclear magnetic resonance is in medical imaging. Typically, the resonance of protons are used to map the distribution of hydrogen in the imaged object. The information is gathered in two dimensions and sorted using Fourier analysis to produce an image. Lately, an interest in functional imaging have risen. In this case, researchers try to map the distribution of specific metabolites like carbon and phosphate in order to infer information about the functional state of an organ. This section is concerned with developing an understanding of the basic principles of NMR. First, We discuss the physical basis of NMR

from a classical point of view. Then, we review image acquisition and formation briefly.

2.3.2 Classical Treatment of NMR

An external magnetic field $\overline{B}$ will produce a torque on a nuclear dipole. This torque is equivalent to the rate of change of angular momentum of the nuclear dipole according to the relation

$$\overline{\tau} = \frac{d\overline{J}}{dt} = \overline{\mu} \times \overline{B}$$

where $\overline{J}$ is the angular momentum, and $\overline{\mu}$ is the magnetic moment of the nuclear dipole. The magnetic moment is related to the angular momentum by

$$\overline{\mu} = \gamma \overline{J}$$

where γ is the gyromagnetic ratio. Eliminate $\overline{J}$ to get the classical equation of motion for the precession of the magnetization

$$\frac{d\overline{M}}{dt} = \gamma \overline{M} \times \overline{B}$$

where $\overline{M} = \sum \overline{\mu}$, is the net macroscopic magnetization for the ensemble.

This result can be understood if we realize that a cross product in mathematics correspond to a rotation in the physical world. This equation tells us that at any instant, the changes in $\overline{\mu}$ are perpendicular to both $\overline{\mu}$ and $\overline{B}$. Thus, a large static magnetic field puts a torque on the magnetic moments and the moments rotate, or precess, around the applied magnetic field (Figure 2.4). It follows

30

that an ensemble of spins would inscribe a cone as shown in figure 2.4. A very close classical example for this is the movement of a gyroscope. When one winds a gyroscope and puts it on the floor, it spins and at the same time precesses around a vertical line (i.e. earth gravity is the applied field in this case).
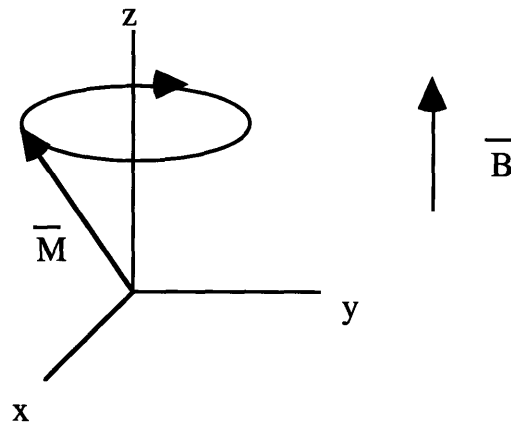
Figure 2.4 The magnetic moment is precessing around the applied magnetic field.

The frequency at which a particle precesses in the presence of a magnetic field is called the Larmour frequency, ω_l. Now conceptually, in order to give energy to the system, we have to apply a field that has component in the x-y plane. Furthermore, this component should time-vary in resonance with the Larmour frequency of the target particle.

The behaviors of the macroscopic magnetization $\overline{M}$ with its components M_x, M_y, and M_z are described by a system of differential equations, the Bloch equations. They describe in simple way many

important experimental results: (1) If magnetization and magnetic field do not have same orientation, the magnetization precesses around the magnetic field. (2) If one waits long enough after a perturbation, equilibrium magnetization is reached; the M_z component parallel to the magnetic field equals M_0 and the transverse components perpendicular to $\overline{B}$ vanish. The exponential approach of M_z to the value of M_0 in Boltzmann equilibrium is described by the following equation:

$$\frac{dM_z}{dt} = \frac{M_0 - M_z}{T_1}$$

where T_1 is called the longitudinal relaxation time. The decay of the transverse components is described similarly

$$\frac{dM_{x,y}}{dt} = -\frac{M_{x,y}}{T_2},$$

where T_2 is called the transverse relaxation time. By combining these equations with the classical equation of motion which was derived earlier, one obtains the Bloch equations

$$\frac{dM_x}{dt} = -\gamma(\overline{B} \times \overline{M})_x - \frac{M_x}{T_2}$$

$$\frac{dM_y}{dt} = -\gamma(\overline{B} \times \overline{M})_y - \frac{M_y}{T_2}$$

$$\frac{dM_z}{dt} = -\gamma(\overline{B} \times \overline{M})_z + \frac{M_0 - M_z}{T_1}$$

3 2

To cause transition in the energy levels of the magnetization, an rf field, $\overline{B}_1$, that is linearly polarized perpendicular to the main magnetic field, e.g. in the x-direction, is applied. This applied field can be divided into two circularly polarized alternating components, one clockwise and the other anti clockwise. The total magnetic field in the presence of the rf field is

$$\overline{B} = B_1\cos(\omega t)\overline{i} + B_1\sin(\omega t)\overline{j} + B_o\overline{k}$$

When this is inserted in the Bloch equations we get

$$\frac{dM_x}{dt} = \gamma(M_yB_o + M_zB_1\sin(\omega t)) - \frac{M_x}{T_2}$$

$$\frac{dM_y}{dt} = \gamma(M_zB_1\cos(\omega t) - M_zB_o) - \frac{M_y}{T_2}$$

$$\frac{dM_z}{dt} = \gamma(M_xB_1\sin(\omega t) - M_yB_1\cos(\omega t)) + \frac{M_o - M_z}{T_1}$$

The solution for these equations can be easily derived for special rf pulses. For example

Case 1. After a 90º pulse, at t=0, $\overline{M} = (M_x(0),0,0)$, solution of the Bloch equations gives

$$M_x(t) = M_x(0)e^{-t/T_2}\cos(wt)$$

$$M_y(t) = M_x(0)e^{-t/T_2}\sin(wt)$$

$$M_z(t) = M_o(1 - e^{-t/T_1})$$

In this case the macroscopic magnetic moment will precess in the x-y plane. It will decay with two time constants, T_1, and T_2. The spin-spin, or transverse, time constant, T_2, is the time constant for the dephasing of the individual magnetic moments of the sample. If a proper coil is used, a signal will be recorded. This signal is called the Free Induction Decay (FID) (Figure 2.5). When these moments are out of phase, they sum destructively and the signal disappears, $M_x = M_y = 0$. Note that in figure 2.5 the spins are drawn in the rotating reference frame, axes are primed. In such frame of reference, the observer is rotating with the spins at some frequency, the Larmour frequency in this example. Thus the spins appear to be constant (i.e. not rotating). Also note that we use T^*_2 instead of T_2. This is because of the field inhomogeneity in the magnet. This is given by

$$\frac{1}{T^*_2} = \frac{1}{T_2} + \frac{\gamma \Delta B_O}{2}$$

where ΔB_O is the field inhomogeneity.
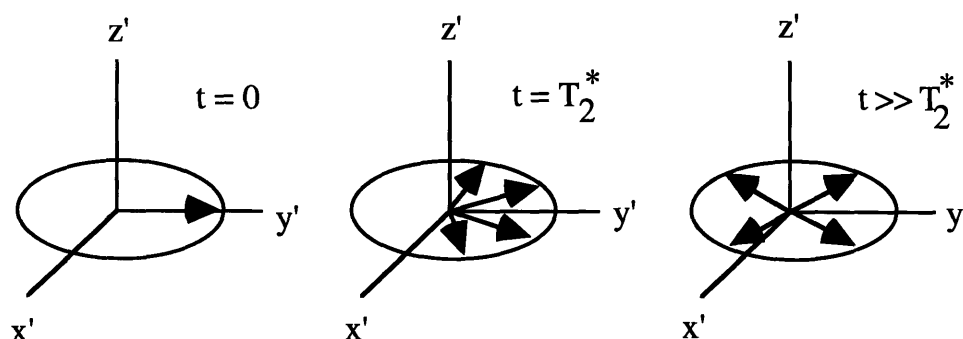
Figure 2.5 Spin-Spin relaxation, T_2.

On the other hand, the spin-lattice, or longitudinal, time constant, T1, describes the rebirth of the equilibrium magnetization, $M_z = M_o$.
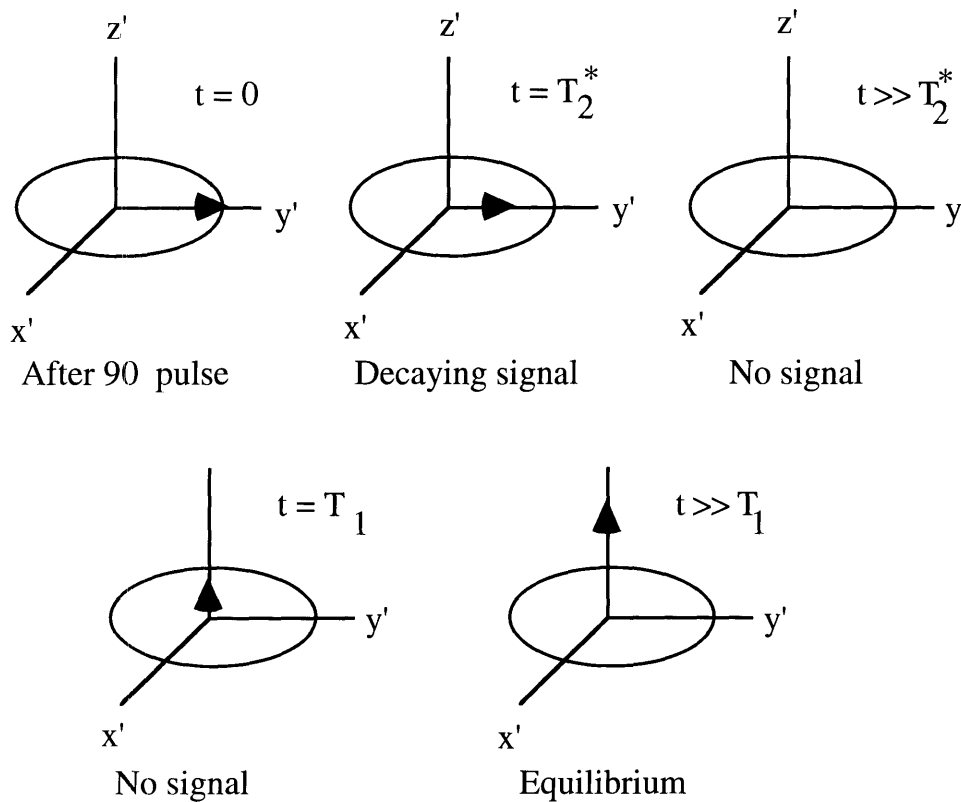
Figure 2.6 Evolution of the spins as a function of time after a 90° pulse. When the spins are dephased in the x-y plane, no signal is induced in the receiver coil.

Case 2. After a 180° at t=0, $\overline{M} = (0,0,-M_o)$, solution of the Bloch equation gives

$$M_x(t) = 0$$

$$M_y(t) = 0$$

$$M_z(t) = M_O(1 - 2e^{-t/T_1})$$

The evolution of the spins after this pulse is shown in figure 2.6.

2.3.3 Spin Echos

Different spin sequences have been developed for NMR. We will describe in this section a spin sequence called the Carr-Purcell and Meiboom-Gill (CPMG) technique. This is a widely used sequence for medical imaging and it will be described briefly. Interested readers should consult the references for more detailed treatment of spin sequences.

The CPMG consists of

$$90_{x'} - \tau - 180_{y'}$$

As shown in figure 2.7, the $90_{x'}$ pulse flips the spins around the x-axis onto the y-axis. After a later time, a $180_{y'}$ refocusing pulse is applied along the y-axis. The refocusing pulse flips the spins around the y-axis by 180°. This reverses the location of the spins so that the spins that were rotating clockwise are rotating counter clockwise towards the y-axis. On the other hand, spins that were originally rotating counter clockwise are rotating clockwise towards the y-axis. As a result of this, at time 2τ later, the spins are refocused along the y-axis and a FID is observer.

36
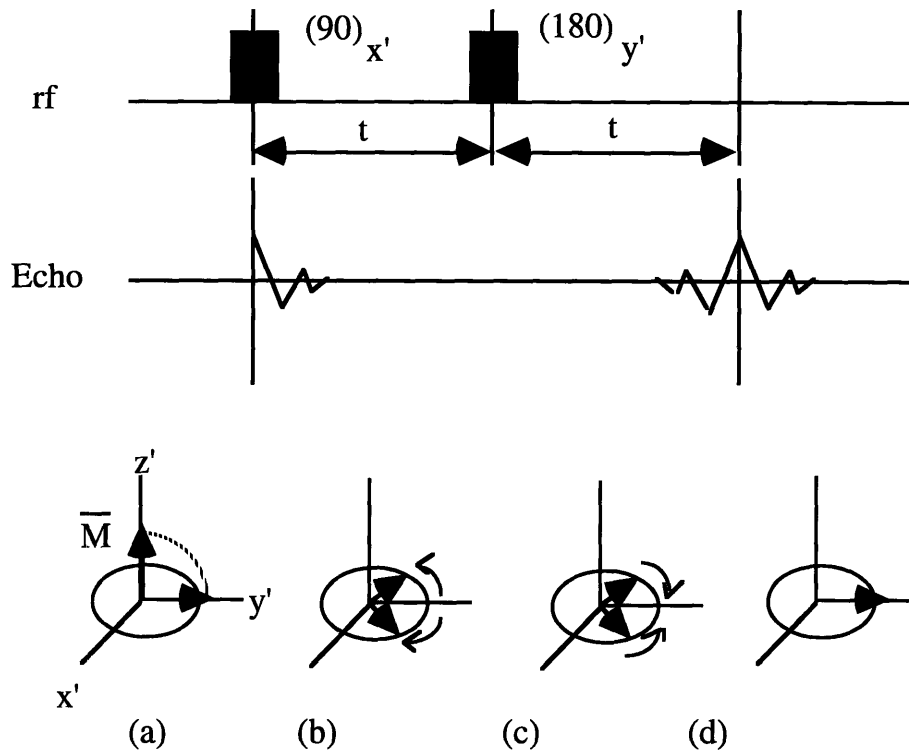
Figure 2.7 The CPMG sequence. a) a 90° pulse flips the spins onto the y-axis. b) The spins dephase losing the signal. c) a 180° pulse cause the spins to refocus. d) an echo appears at 2t.

The CPMG sequence is commonly used in MRI. A typical imaging sequence is show in figure 2.8. A gradient in the z-axis and a soft rf pulse are used for slice selection. The image matrix is frequency encoded in the x-axis and phase encoded in the y-axis. The phase encoding is repeated with incrementally increasing gradients as shown in the figure 2.8. The repetition time is called TR, "time to repeat". A 180° pulse is used for refocusing and the echo occurs at TE/2 later, where TE is "time to echo". The recorded signal from slice at $(z = z_0)$ is

$$S(t_x, t_y) = M_O \iint \rho(x, y, z = z_o) \exp\left[-i\gamma\left(x g_x t_x + y G_y T_y\right)\right] dx dy$$

where

M_O is the thermal equilibrium magnetization,

$\rho(x, y, z = z_O)$ is the density of spins at (x,y) in slice at z= z_0,

G_x is the gradient strength in the x-axis (frequency encoding

gradient or readout gradient),

G_y is the gradient strength in the y-axis (phase encoding), and

T_y is the duration of a phase encoding step.

In the above equation, it was assumed that $\rho(x, y, z = z_O)$ included the T1 and T2 decays. Hence the spin density function is modulated by the relaxation times. A more explicit form for the spin density function is

$$\rho(x, y, z = z_O) = \rho_O(x, y, z = z_O) \left\{ \exp\left[\frac{-T_E}{T_2(x, y, z_O)}\right] \right\} \left\{ 1 - \exp\left[\frac{-T_R}{T_1(x, y, z_O)}\right] \right\}$$

where

$\rho_O(x, y, z = z_O)$ is the initial spin density at location (x, y, z_0),

TE is the time to echo, and

TR is time to repeat.
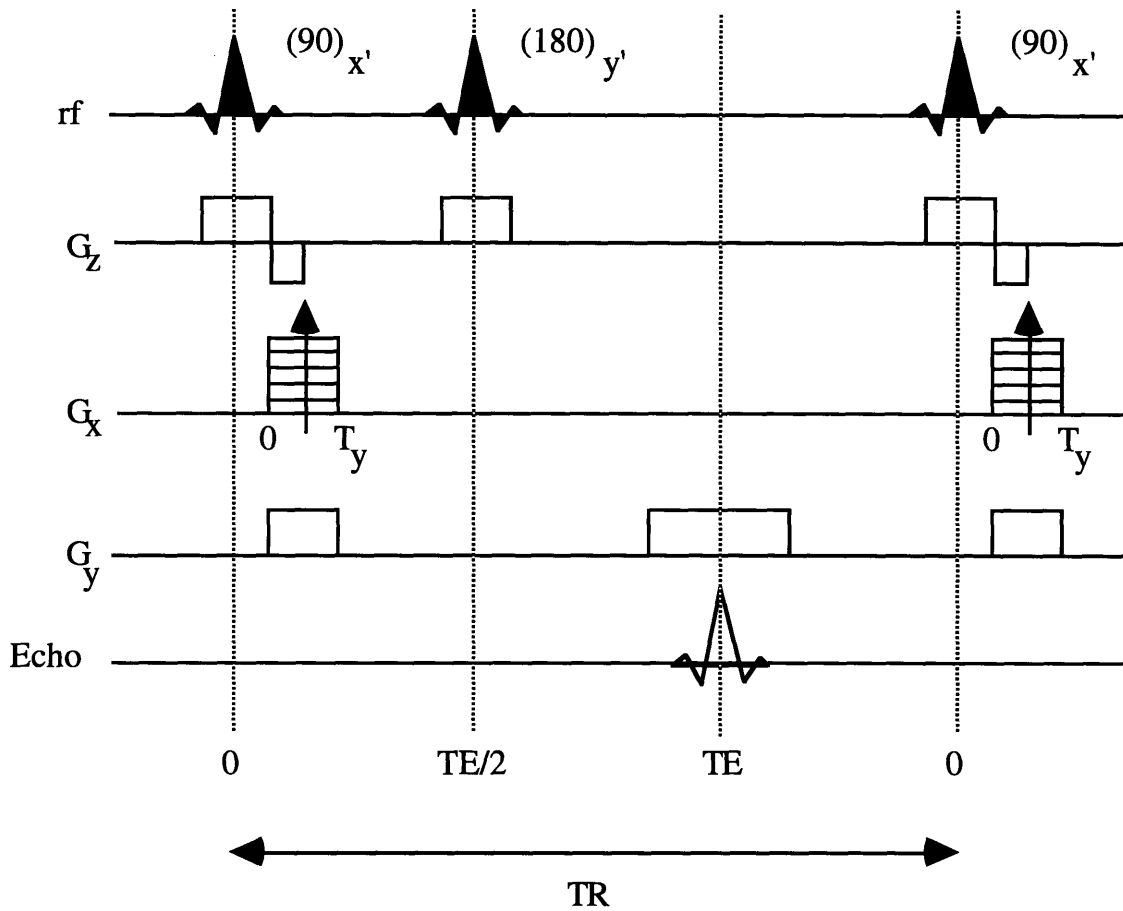
Figure 2.8 Pulse sequence for 2-D spin echo Fourier imaging.

The concepts involved in image acquisition will be discussed in the following section.

2.3.4 Conclusion

MRI is sensitive to differences in the density of spins, e.g. protons in most cases. The images can be made to reflect the relaxation times of the spins in the region of interest. Images formed this way are normally called T_1 and T_2 weighted images. For example, figure 2.9 shows a T_2 weighted image for the brain. From the previous

discussion of NMR principles, it should be clear that no functional information are contained in MRI explicitly. Function is only reflected through the anatomy. Although functional MRI is an area of active research, at present, clinical MRI relies mostly on anatomical information. Thus, registration with a functional based modality, e.g. SPECT, is very desirable for the reasons outlined briefly in Chap. 1.
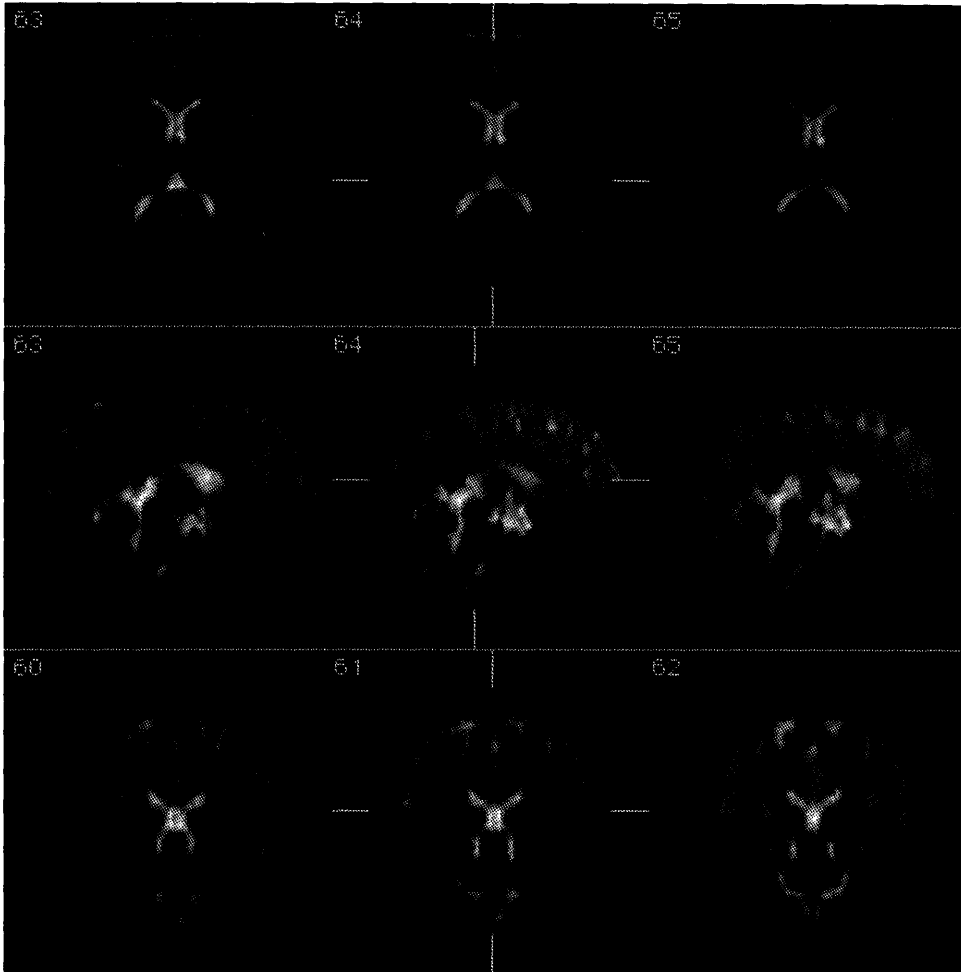
Figure 2.9 Example of a T_2 weighted image of the brain. Note the lower resolution of the sagittal and coronal planes. This is because the image was acquired axially with slice thickness of 5mm. and no gap.

Chapter 3

*When I was a boy of fourteen, my father was so
ignorant I could hardly stand to have the old man
around. But when I got to be twenty-one, I was
astonished at how much the old man had learned in
seven years.*

— Mark Twain

Overview of Image Registration Algorithms

We are concerned with the registration of 3-D medical images of the
brain extracted using SPECT, and MRI. In such cases two 3-D images,
a reference image and an active image, are used. Once aligned, the
reference image is fixed in space while the active image is
transformed geometrically until it is registered to the reference
image. Geometrical transformation in this context includes
translation, rotation, and scaling only. Different techniques have
been developed for the registration of medical images. Most
registration techniques following the general registration frame
outlined in Chapter 1.3, undergo similar steps: firstly extracting
image features, then estimating a registration transform, finally
calculating a quality of fit figure. In general, the goal of registration
is to find a registration transform that optimizes the quality figure
for each set of images. Thus the last two steps of registration,
estimating a registration transform and calculating the quality figure,
are repeated iteratively until a satisfactory registration is achieved.

Extracting image features play a fundamental rule in registration. The way a specific registration technique utilizes these features to estimate the registration transform ultimately decides the success of the registration method. We have in Chapter 1.3 classified image registration techniques based on the type of features they extract from images. We introduced four broad classes: registration using external markers, surface registration, analytical registration, and volume registration. These methods vary in their stability depending on the amount of information incorporated in the registration process. Furthermore, in practical applications, other considerations like numerical efficiency and easiness of operation apply to image registration techniques. In this chapter we describe some commonly used registration methods. We also discuss some strong and weak points of these methods. For more details, interested readers should consult the references.

3.1 External markers

This is the simplest and most straight forward registration method. It relies on the existence of visible external fiducial markers on both images, the active and the reference images.

3.1.1 Registration using external markers

Image registration using external markers consists of three steps. The first step is to identify the locations of the markers in 3-D on both of the image sets. This is done manually by an operator who views the images in 3-D and selects the fiducial points using a

pointing device. Fiducial markers appear on the image as sphere or a cylinder of activity that cover a number of pixels depending on the pixel size, the shape of the marker, and the resolution of the imaging modality. Therefore, the operator has to identify the center of the marker. This could be done manually be choosing the pixel with the highest activity in 3-D. Another implementation allows the user to draw a region of interest around the marker. The computer, then, fits a gaussian to the points inside the region of interest and the center is calculated.

The second step is to use these points to calculate a transformation matrix that will match the coordinates of one set of markers to the other. The transformation may have the following general solution

$$P' = R * ((P * S) - C) + T,$$

where

P is the input point vector (x, y, z),

P' is the transformed point vector,

R is the 3x3 transformation matrix,

C is the translation matrix for the center of rotation, and

T is the translation matrix.

The transformation is either calculated analytically or is estimated iteratively. In the former case, an operator has to identify each marker on the active image and its corresponding marker on the reference image. In the later case, the operator defines the location of all the markers on both images and the computer estimates the

best geometrical transformation that matches the coordinates of the marker sets. In order for this method to work, the object, defined by the markers, is treated as a rigid body for which the relation between the markers has to conserved. The accuracy of registration is commonly quoted as the root mean square error of the 3-D distance between the transformed points and the targeted points:

$$Err = \sqrt{\frac{1}{N}\sum_{1}^{N}\left(P1_i - P2'_i\right)^2},$$

where

$P1_i$ is the position of the ith marker on the first image,

$P2'_i$ is the transformed position of the ith marker on the second image, and

N is the number of markers.

The final step in the registration process is to use this transformation matrix to reformat geometrically the data set of the active image with respect to the data set of the reference set.

3.1.2 Difficulties with external markers

Difficulties with using external markers for registration is two folds, the design of the markers, and the positioning of the markers. The markers have to be visible on both data sets, reference and active. When more than one imaging modality is used, special care has to be taken in the design of the markers. For example, in the case of SPECT and MRI registration, the markers have to be radioactive so that they are visible on SPECT and they must contain

water (or a compound rich with hydrogen) so that they are visible on MRI. Our group has designed small cylindrical markers (few millimeters on the side) that contained two compartments. One was filled with Cobalt-60 and the other contained water. These markers were visible clearly on both MRI and SPECT.

Another aspect in the design of markers is the intensity of their signal. The signal from the markers has to be low relative to neighboring tissues so that the signal from neighboring tissues is visible and not smeared out. This can be solved on planar scans by positioning the markers far a way from any region of interest. However, in tomographic imaging, the effect of high signal markers can not be isolated and may introduce artifacts in the image. The obvious solution to this problem is to make the radioactivity and the amount of water inside the markers as small as possible with out losing the signal on the final image.

Some care has to be taken in the imaging of markers. Usually, markers are designed to be as small as possible. Generally speaking, markers are smaller than the resolution limit of SPECT. Which means that a new high signal, high frequency component is introduced in the object. This may require more processing. For example, more projections are required for the tomographic image, and the projections need to be processed with a low pass filter before reconstruction. If this is not done adequately, star artifacts may be visible surrounding the marker location. In the extreme case, these artifacts could significantly compromise the quality of the image.

The other issue which makes the use of external markers cumbersome is the positioning of the markers. The markers have to be positioned on the object such that they are visible in the image. They have to be stationary during the acquisition of the image. They have to be fixed firmly so that they do not move between images in which cases the patient may have to be transported to a different scanner, e.g. move from nuclear medicine lab to MRI lab. Finally, the marker positioning must be reproducible for subsequent scans which could be days or weeks later. Many techniques have been suggested and tried to solve some of these problems, none of which is completely satisfactory. We describe here three approaches: fixed stereotactic frames, temporary point markers, and molds and head masks.

i) Fixed stereotactic frames

These are frames that are fixed to the head with screws that are drilled in the skull. This is commonly used for radiation therapy planning where the therapy routine is done first on an x-ray simulator. The location of the tumor is defined with respect to the frame in 3-D. Later the actual radiation dose is delivered to the tumor in the frame reference coordinates. Lately, other modalities have been used to better diagnose and measure the extent of the tumor. For example, special markers have been designed to show on MRI and positron emission tomography (PET). These markers are fixed to the stereotactic frame which is fixed to the skull. The

combined registered images from CT, MRI, and/or PET is analyzed and the treatment procedure is planned.

Stereotactic frames, or the screws that hold them, are fixed on the skull for the duration of the treatment which could last for days or weeks. This type of referencing is crucial for radiation therapy, due to its spatial accuracy. However, it is difficult to justify it for routine diagnostic use.

ii) Temporary point markers

These are of the type described previously. They are small cylindrical containers which contain an agent that is visible on the imaging modality, e.g. radioisotope for SPECT/PET or water for MRI (Erickson 1993). These markers are fixed to the head with a tape or a band. They are not well fixed and susceptible to movement. Therefore special care has to be taken to keep them from moving during or between scans. Also, repositioning these markers in the same locations after they have been moved is usually very difficult. Therefore, reproducibility is a big concern when this type of markers is used.

iii) Molds and head masks

Using molds and head masks to fix the markers was developed as a compromise between the above two methods. It provides less drastic intervention than the fixed frames, no screws in the skull. Also, the markers are less susceptible to movement than the single point markers. The molds are shaped on the head of the patient.

They conform to the shape of the head and can be fixed so that they fit the head in a specific orientation. Therefore, positioning can be reproduced with reasonable accuracy. Point markers are fixed on top of the molds in a similar way to the fixed frames (Shukla 1992).

Making molds and head masks require special expertise. The patients have to be fitted and the molds have to be cast. This requires extra time and expense and is cumbersome for regular routine examinations. Also, the molds are not comfortable to wear for extended times. Finally, in some cases where the patient is unconscious, it is difficult to make and fit the molds.

3.1.3   Conclusion

Although very accurate registration using external markers is achievable, the difficulties involved make such an approach undesirable. These difficulties arise from the extra care that is required in building, positioning, and imaging these markers. Also, when external markers are used, only scans that have these markers with exact positioning can be registered. This excludes previous scans which did not have the same markers and scans that were done at other institutions. Clearly it is more desirable and practical to have registration methods which rely on internal structural markers, e.g. anatomical features, or some inherent properties of the imaged objects, e.g. volume or surface, to do the registration. Some examples of these registration methods will be discussed in the following sections.

3.2 Analytical registration

Analytical registration is based on the calculation of the moments and their derivatives of the object under consideration. Two sets of calculations are necessary, one for the active image and one for the reference image. These values can be used to calculate an exact analytical solution, as opposed to iterative solutions, to the registration function. A notable example is registration using the principal axis transformation (Alpert 1990).

3.2.1 Principal axes transformation

This technique assumes that the head can be treated as a rigid body which is uniquely located by knowledge of the position of its center of mass and its orientation (rotation) with respect to the center of mass. The center of mass, inertia matrix, and principal axes can be determined for any rigid body. Surface or volume models are derived for the reference and active images by interpolating edge contours drawn on serial axial slices of the corresponding images. It has been found that volume models give more robust registration than surface models (Alpert 1990). When two models are used for the same object, the centers of mass for the models will represent the same physical point in the object, independent of the orientation or scale. The center of mass is

$$[\bar{x},\bar{y},\bar{z}] = Mean([x,y,z]),$$

where x, y, z are the integer coordinates of an image voxel and the symbol *Mean* indicates the arithmetic mean over the set of reference voxels coordinates.

The scale difference can be calculated and corrected for by knowledge of the pixel size of both images. The translational displacement of the two volumes can be determined from the center of masses, using the zero-order and first-order moments:

$$[x',y',z'] = [x,y,z] - [\bar{x},\bar{y},\bar{z}],$$

where [x, y, z] and [x', y', z'] are the old and new coordinates of each point.

The inertia matrices I_i, for the two volumes can be expressed as a similarity transformation:

$$I_i = S_i I S_i^T,$$

were i is for reference or active images, I is the inertia matrix computed in the principal axis coordinate system and the rotation matrix, S_i, is the matrix of the eigen columns, orthonormal vectors directed along the principal axes, determined from I_i. Geometrically, the above equation can be interpreted as a rotation of the I relative to the original image coordinate axes. The inertia matrices for the reference and active volumes, I_1 and I_2, are related by

51

$$I_2 = S_2 S_1^T I_1 S_1 S_2^T,$$

were the inner product recovers the inertia matrix in the principal
axis coordinate, I. Thus registration between image 1 and image 2
can be obtained by a translation to the center of mass coordinate
system followed by the rotation $S_1 S_2^T$.

3.2.2 Conclusion

Generally speaking, registration using moments does not behave
reliably in the case of noisy or incomplete data. Also, the success of
registration is dependent significantly on the ability to delineate
exactly corresponding volumes in the two image sets. This is
problematic with images that represent different information, e.g.
functional vs. anatomical images (Rusinek 1993).

3.3 Surface registration

Surface fitting methods are based on the assumption that the head
can be treated as a rigid body. For such a case, given two 3-D models
of a head, a unique coordinate transformation can be found which,
when applied to one of the models, makes the two fit together most
closely. Surface registration involves deriving a 3-D surface model of
the organ to be registered. It is typically accomplished by
interpolating edge contours drawn on transverse slices of the organ.
The surface of the active image is iteratively translated, rotated and

scaled to match the surface of the reference image. Matching is defined by optimizing a quality of fit figure, e.g. distance between surfaces. When the surfaces are registered, the final registration transform is applied to the original data of the active image. Finally, the registration is validated by an expert's inspection.

3-D surface registration was introduced and pioneered at the University of Chicago and an algorithm called "head and hat" was developed. The general features of this algorithm are described in the following section. Also, another algorithm, the chamfer matching, is presented as a modification to 3-D surface registration which accelerates the optimization process. (Pelizzari, 1989 ; Barrow, 1977)

3.3.1 The "Head and Hat" Algorithm

The "head" and "hat" data sets correspond to the reference and active images respectively. The principle of fitting is simple, analogous to the optimum placement of a custom fitted, rigid hat onto a head. Obviously, this method would not work for highly symmetric objects. However, perfect symmetry is sufficiently lacking in human heads that surface fitting may succeed if an adequate surface model of the head is used.

Registration using the "head and hat" algorithm consists of multiple stages; first, the 3-D surface models of the "head" and the "hat" are produced. This is done by interpolating surface contours drawn on the serial slices of each scan. Transverse slices are commonly used for this purpose. The "head" model is a stack of disks or "prisms"

(Siddon 1985) from one image with thickness and vertical position appropriate to the slice in which the contour was made. The "hat" model is represented as a set of independent points lying on a set of parallel planes from the other image. These parallel planes correspond to the parallel transverse planes of the contours and of no further interest once the 3-D coordinates of the points have been generated.

The second stage is to use a minimization algorithm to find the geometric transformation that, when applied to the "hat" coordinates, achieves best fit. The quality of fit is estimated using the mean squared distance between "hat" points and "head" surface. This distance is evaluated for each "hat" point by finding the intersection with the "head" surface of a ray from the transformed "hat" point to the centroid of the "head" model. The squared distances from the "hat" points to their intersections are added to calculate the total degree of misfit.

Once the optimum fit is found, the registration transform is applied to the image data corresponding to the "hat" model, active image using our earlier definition. The final stage is to validate the quality of registration visually. This is done by an expert who matches all the slices of the image set.

3.3.2 Chamfer Algorithm

In the "head and hat" algorithm, the error function is determined from the distance between each "hat" point and the "head" surface a

long a ray tracing connecting the "hat" point with the centroid of the "head". The error value is calculated after each iteration. This is a time consuming process which slows down the algorithm significantly. The Chamfer algorithm is an efficient alternative which uses a distance transformation to calculate the error function (Barrow 1977, Jiang 1992). Distance transformation is a process which converts a binary surface image into a gray-level image where all voxels have a value corresponding to the distance to the nearest surface voxel (Borgefors 1990). Using this map as a lookup table, determining the distance from a "hat" point to the "head" surface is just looking at the value of the distance map at the "hat" point coordinates. Distance transformation is applied on the "head" data only.

3.3.3 Conclusion

3-D surface registration algorithms are limited to edge information and do not incorporate information about the internal structures of the organ. As a result of this, they are sensitive to errors in defining edge contours. Also, these algorithms assume that the best registration is achieved at the point where the error function reaches the global minimum. This assumption is true if two conditions are satisfied. First, if there is only one global minimum point in the error function. This is not generally true. In fact often the error function is not simply concave and the gradient-based minimization approach can be easily trapped in a local minimum. Human monitoring and intervention of the fitting process is needed to avoid such trapping. The second condition is if every sampled active/hat surface point has

a corresponding point existing on the reference/head surface. This condition may or may not be satisfied depending on image acquisition and the surface extraction technique. In many cases, especially in multi-modalities imaging, the active volume may have some extra components because of the noise in the image or simply because of the uncorrespondence of function to anatomy if functional and anatomical images are used.

3.4 Volume registration

Volume registration relies on optimizing a function of the values of the corresponding pixels of the active and the reference images. For example, standard data comparison algorithms have been applied to the registration of medical images, e.g., sum of absolute value difference (SAVD), correlation function (CF), and correlation coefficient (CC) (Junk 1990, Bacharach 1992). Other algorithms have been derived specifically for image comparison, e.g., stochastic sign change (SSC), deterministic sign change (DSC) (Venot 1984, Hoh 1993, Minoshima 1992)). These algorithms vary significantly in their complexity and computational requirements. We describe here an algorithm that uses the uniformity of pixel values in corresponding regions of the active and reference images. This algorithm was initially proposed for PET to PET registration, and later modified for PET to MRI registration (Woods 1992, Woods 1993).

3.4.1 PET to PET Registration

Registration is based on the idealized assumption that if two image sets are accurately aligned, then the value of any voxel in one image set is related to the value of the corresponding voxel in the other image set be a signal multiplicative factor, R. If the image sets are misaligned, this multiplicative factor is no longer constant but varies from voxel to voxel throughout the image. The alignment algorithm systematically moves the two image sets relative to one another until this voxel-to-voxel variation is minimized. To make this more explicit, assume that we have two images, an active and a reference images. If a_i is the value of voxel i in the reference image and b_i is value of voxel i in the active image, then $r_i = a_i/b_i$ is the ratio of the values of the two voxels. Assume that r_{mean} is the mean values of the ratios over all voxels within the images and σ_r is the standard deviation of r_i over all voxels of the images. The algorithm uses σ_r / r_{mean} as a measure of how well the two image sets are registered.

The program searches for the best registration parameters (three translations, x, y, z, and three rotations) iteratively. The steepest descent method is used in which the derivative of the ratio σ_r / r_{mean} is calculated after each iteration. The value of the registration parameters that maximizes the first partial derivative is chosen. Convergence is defined as the point at which all of the first partial derivatives fall below a threshold value. In which case, the program is assumed to have reached the lowest point, minima, of the error function surface.

3.4.2 MRI to PET Registration

It was assumed in the previous section that single modality images look a like, PET images of the same subject are similar after alignment and adjustment for pixel intensity. This assumption does not hold for images acquired with different modalities. For example, white matter structures will appear bright on a T1-weighted MRI study and dark on a PET study obtained using [18F]fluorodeoxy-glucose (FDG). Therefore, a new criteria will have to be used for multi-modalities image registration. In this case, it is assumed that all pixels with a particular MRI pixel value represent the same tissue type so that the values of corresponding PET pixels should also be similar to each other.

The MR image is edited manually to exclude nonbrain structures (e.g., scalp, skull, meninges) prior to registration. Then, the MR image is partitioned into 256 separate components based on the value of the MR pixels. Finally, the uniformity of the PET pixel values in each MR partition is maximized by iteratively minimizing a weighted average of the standard deviation of the PET pixel values within each MR partition.

The criteria of fitting is defined as follows; for any voxel i with value j in the MRI study, let a_{ij} be the value of the corresponding PET voxel. Let σ_j be the standard deviation of a_{ij} for all voxels i with an MRI voxel value of j; let a_j be the mean of a_{ij} for all voxels i with an MRI voxel value j, and let $\sigma'_j = \sigma_j / a'_j$. If n_i is the total number of voxels within the image with an MRI value of j and $N = \sum_j n_j$ then

$$\sigma'' = \Sigma_j \sigma'_j \times \frac{n_j}{N},$$

is the weighted average of the normalized standard deviations measured for the various MRI voxel values j. The rest of the algorithm is similar to the PET-to-PET registration described in the previous section.

3.4.3 Conclusion

In reality, even perfectly aligned datasets will still show some residual variation due to counting statistics, partial volume effects, and biological variation. This will introduce inherent limitations to this algorithm. Also, the computational cost is very high.

3.5 Conclusion

Few weak points are shared among most of the registration approaches that were described in the previous sections. First is the lack of control of the operator over the registration procedure. Occasionally, an obvious shift or translation is apparent on the images when they are inspected by a trained operator. These slight misregistrations cannot be corrected directly, because the source of the error is not easily isolated. For, example, the edge contours may not be drawn tight enough, the models for the "head" and "hat" may not be accurate enough, the volumes or structures of the active and reference studies may not correspond due to error on part of the

operator or due to a disease process, or the program might be simply stuck in a local minima. These uncertainties may result in long hours of frustrated bug hunting or a failure in registration.

Second, the previous algorithms are designed for the registration of two studies. They can not be used to align a single study. We will visit this point in the following chapter. Finally, registration of ^{201}Tl-SPECT with perfusion SPECT or MRI is unachievable using the previous methods. This shortcoming is significant considering that ^{201}Tl-SPECT lacks localization information and requires registration with anatomical modalities.

We have developed a robust registration approach, called ALIGN, that differs from most other registration techniques in that it allows the user to incorporate all of the available information within the images in the registration process. Consequently, it is potentially more stable than other techniques. This method separates the 3-D registration problem into three, 2-D sub-problems, each of which is tractable. The overall effect is a registration algorithm that is easy to implement and can achieve accuracy on the order of a pixel. The following chapter describes the implementation of our method, and explains why (because of the redundancy of information in the three 2-D images) it is ideal for the registration of noisy images such as those produced by SPECT.

Chapter 4

A law of nature rules that energy cannot be destroyed. You change its form from coal to steam, from steam to power in the turbine, but you do not destroy energy. In the same way, another law overruns human activity and rules that honest effort cannot be lost, but that some day the proper benefits will be forthcoming.

— Paul Speicher

Materials and Methods

4.1 Acquisition

SPECT images were acquired using a triple detector system (MultiSPECT 3, Siemens Gammasonics Inc., Hoffman Estates, Ill.). Typically, 120 projections of 128 x 128 pixels at 3-degree intervals were acquired. Image reconstruction was accomplished using the back projection algorithm with a Butterworth filter (cutoff = 0.45; order = 5). A total of 128 consecutive slices of 2.45 mm. thickness were reconstructed in 128 x 128 matrix with pixel size of 2.45 x 2.45 mm. for each study. The Chang method for attenuation correction (Att. factor = 1.2) was applied on the images. Standard nuclear medicine software was used in the acquisition and reconstruction of the data (ICON, Siemens Gammasonics Inc., Hoffman Estate, Ill.).

MRI data were acquired using a 1.5 Tesla device (Signa Scanner, GE Corp., Milwakee, Wis.). Typically, studies consisted of 18 slices of

256 x 256 pixels with slice thickness of 3 mm. and gaps of 5 mm. between slices. Pixel size was 0.94 x 0.94 mm. for most of the studies. MRI studies were transferred through the hospital network to the nuclear medicine computer system.

Slices from SPECT were stacked into a data cube of 128 pixels on the side (voxel size 2.45 x 2.45 x 2.45 mm.). In the case of MRI, in which 18 slices were typically acquired, slices were resampled and interpolated to match the SPECT format. All the transformation and manipulation of data were performed on the nuclear medicine system.

4.2   Registration

4.2.1   Alignment of a single study

The purpose of this feature is to align the organ under investigation, e.g. the brain, according to some standard orientation. In the case of the brain, this is important clinically because it emphasizes left/right hemisphere symmetry/asymmetry and facilitates comparison to a standard anatomical atlas. Figure 4.1 shows an ALIGN page for single study alignment.

A single study, active study, is selected. Three (128 x 128 pixels) slices of orthogonal planes through the data stack of the study are displayed. In the case of the brain, these slices correspond to transverse, coronal, and sagittal sections. These orthogonal planes

62

show the location and orientation of the study with respect to the axes of the data cube.

The operator selects one plane (transverse, coronal, or sagittal), and the corresponding slice of the selected plane is magnified into a (256 x 256) image. Any slice in the selected plane can be chosen by traversing through the data stack. Tick marks indicate the location of the current slices with respect to the data cube. For example, on the transverse image tick marks indicate the location of current coronal and sagittal slices with respect to the data cube (Figure 4.1).

The selected slice of the study can be translated and rotated. The resultant transformation is propagated through the data stack, and the effect in the other planes (i.e., orthogonal to the selected plane) is displayed in the respective images. This is analogous to moving an object in a box with three orthogonal windows on the sides. Any movement of the object from one window affects the way it appears in the other two windows. The process can be repeated for other planes until the organ orientation in all planes is satisfactory. At this stage the study is resliced and saved with the new orientation.
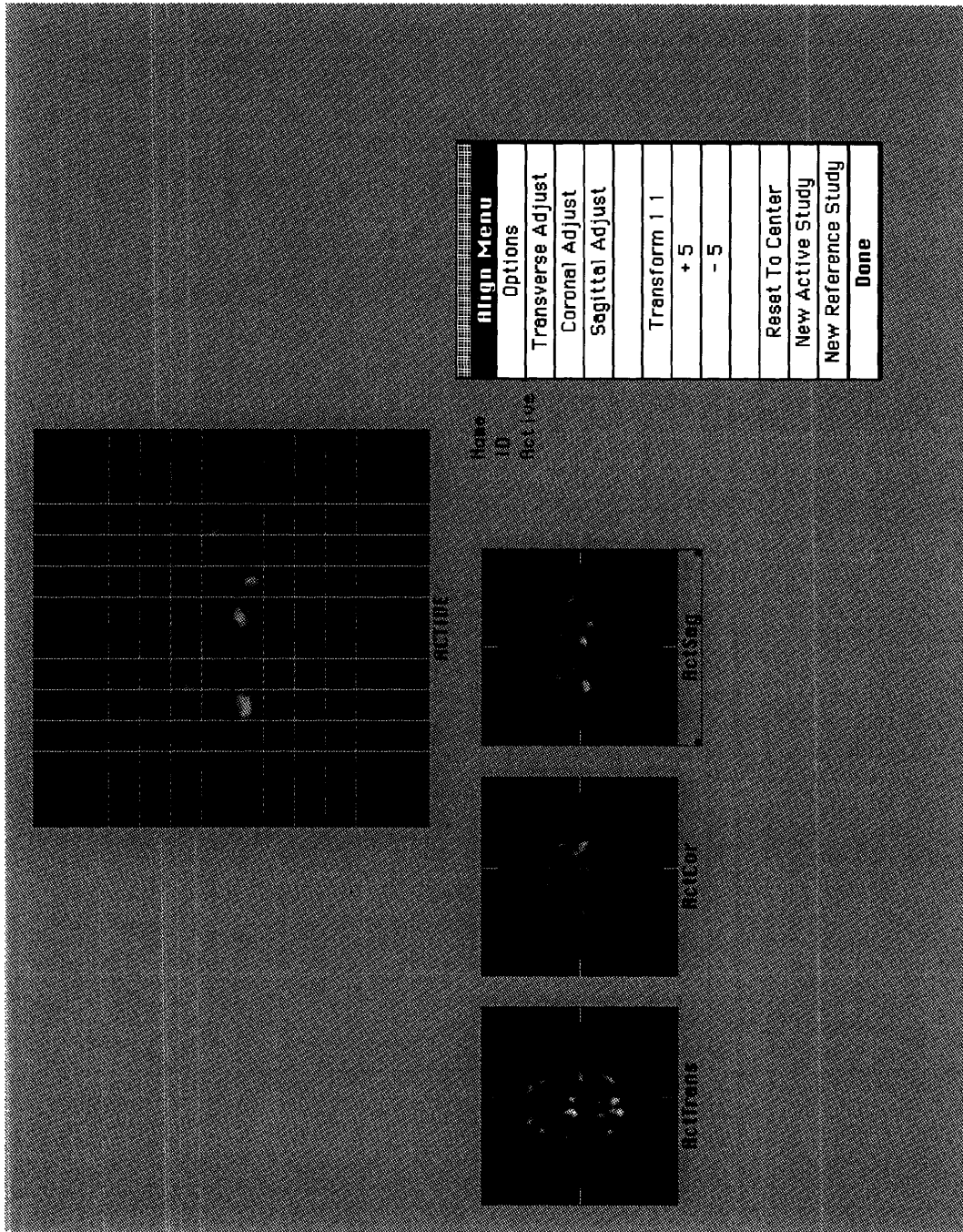
Figure 4.1 Single study alignment. See text for details.

4.2.2 Registration of two studies

Typically, two studies are selected: a reference and an active study. The reference study is kept stationary, and translations and rotations are applied only to the active study. The goal of the registration process is to reorient or register the active study to the coordinates of the reference study.

For each of the active and reference studies, three (128 x 128) slices of orthogonal planes through the corresponding data stack are displayed. These orthogonal planes show the location and orientation of the active study with respect to the axes of the data cube and the reference study.

The operator selects one plane (transverse, coronal, or sagittal), and the corresponding slices of the selected plane from the active and reference studies are magnified into two (256 x 256) images. Any slice in the selected plane can be chosen (Figure 4.2).

The selected slice of the active study can be translated and rotated with respect to the reference slice to match the orientation of the reference slice in the same plane. The resultant transformation is propagated through the active stack, and the effect in the other planes (i.e., orthogonal to the selected plane) is displayed in the respective images. The process is repeated for other planes until slices from both studies, active and reference, match in all planes. When matching occurs in all planes, the studies are said to have been registered. Figure 4.3 shows a flow diagram of ALIGN.
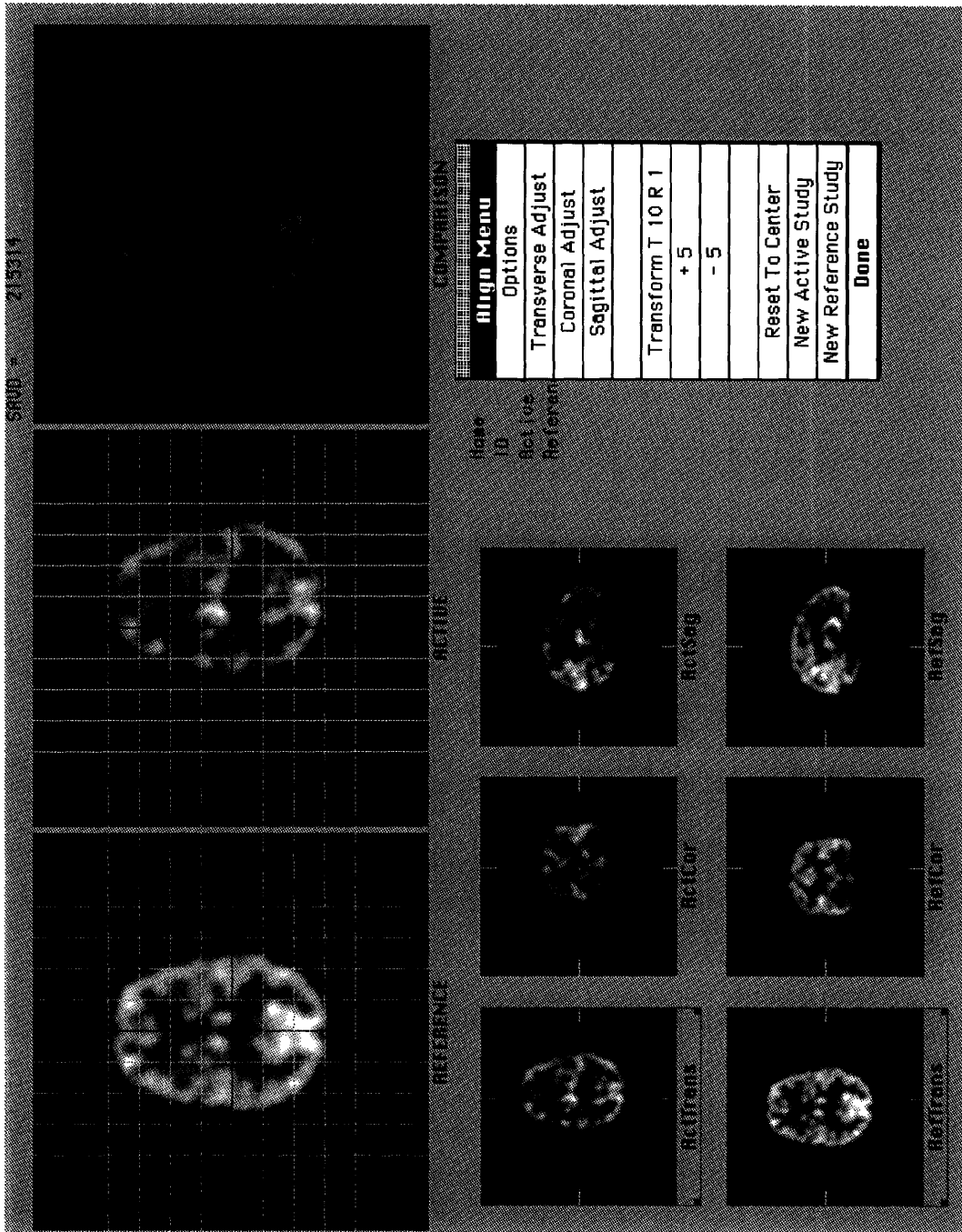
65

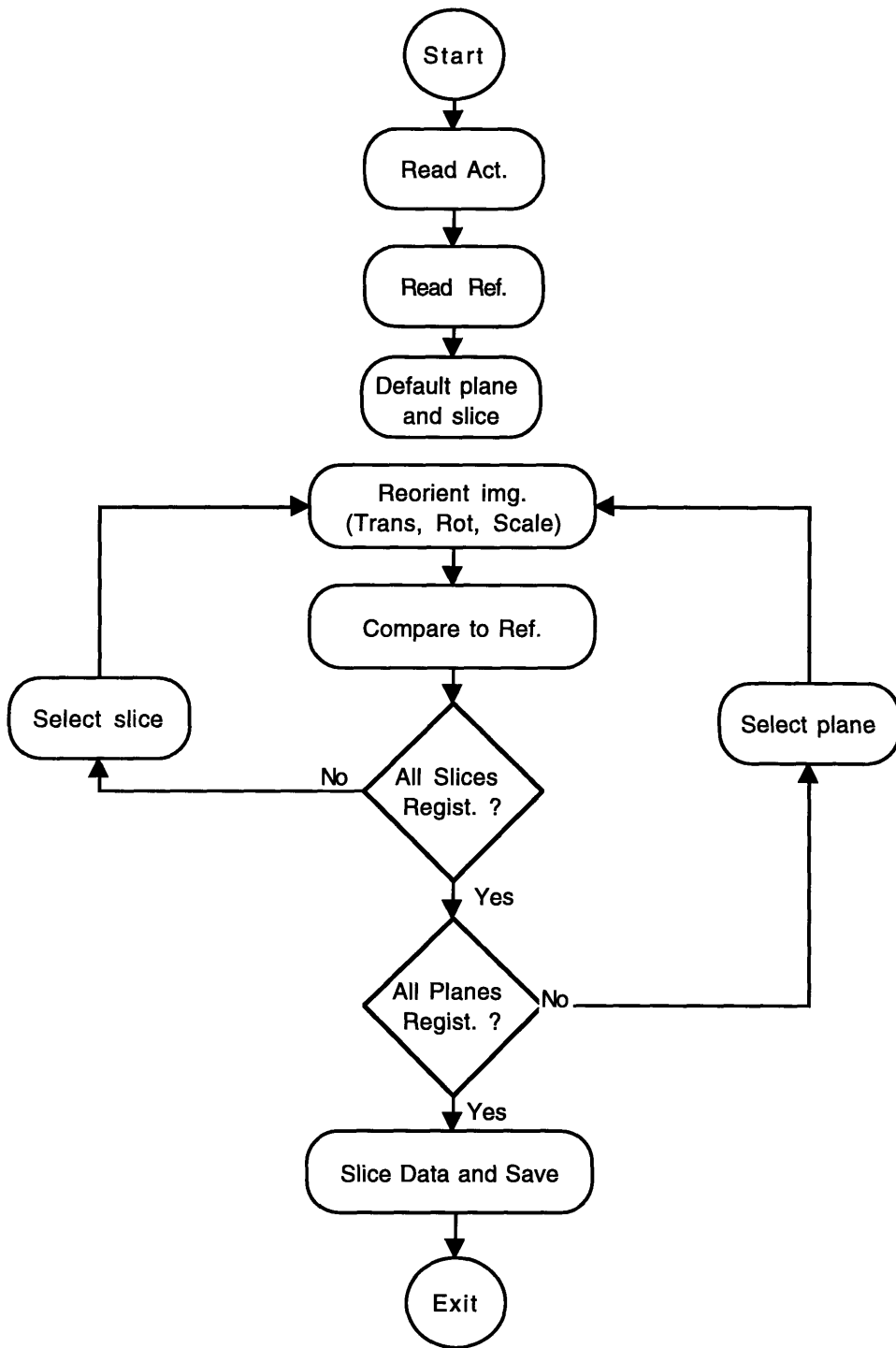**Figure 4.2** Outlines of ALIGN page. See text for details.

66

**Figure 4.3** Flow diagram of ALIGN. See text for details.

Comparison between corresponding slices (e.g., transverse to transverse) is achieved in three ways: alignment of image features on grid lines, the sum of absolute value difference (SAVD) of the active and the reference images, and a comparison window (Figure 4.2). Grid lines are displayed on the 256 x 256 images. These grid lines are defined with respect to the axes of the data cube and are fixed. Therefore, the grids of the two large images are matched and can be used in the alignment of corresponding features of the active and reference slices. The sum of absolute value difference (SAVD) of the active and reference slices is displayed in the upper right corner of ALIGN page. This value is updated after each translation or rotation of the active image. Finally, the comparison window displays a function of the selected slices of the active and reference studies.

The purpose of the comparison window is to improve registration by emphasizing misregistration between the active and reference slices in the selected plane. Three functions have been implemented thus far, a masking algorithm, an edge display, and a dual color fusion (Figure 4.4). The first function is a mask overlay of the active image on the reference image. The mask is defined by a threshold value of the pixels of the active image. Pixels above the threshold are displayed in black, and other pixels are made transparent. Alternatively, only the edges of the active slice can be overlaid on the reference slice. The edges are calculated using an edge detection algorithm. The third option performs a fusion of the active and reference slices in two colors. The fusion is done by taking

alternating pixels from both images. The operator has the option of performing these functions on the reference image with respect to the active image or vice versa.

Transforming the data stack after each translation or rotation requires several computations which would make the program prohibitively slow. To circumvent this difficulty, the data stack is not modified during the application of the program. Instead, only the displayed slices are extracted (three images for each study) in oblique planes that correspond to the transformation parameters.
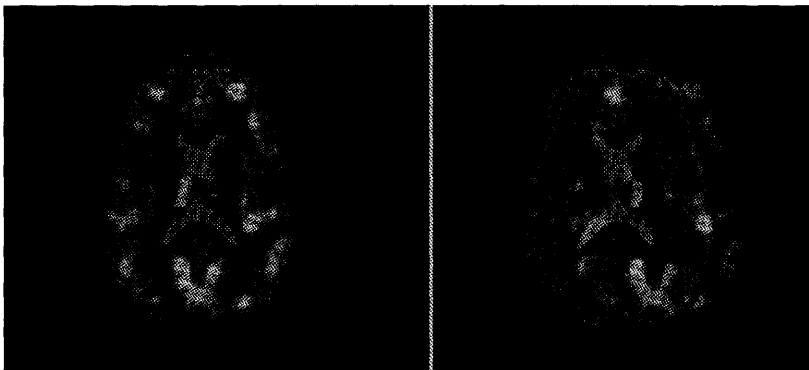
a)
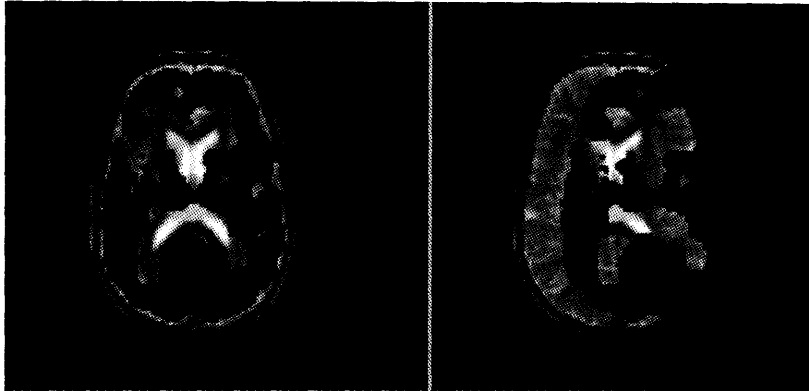
b)
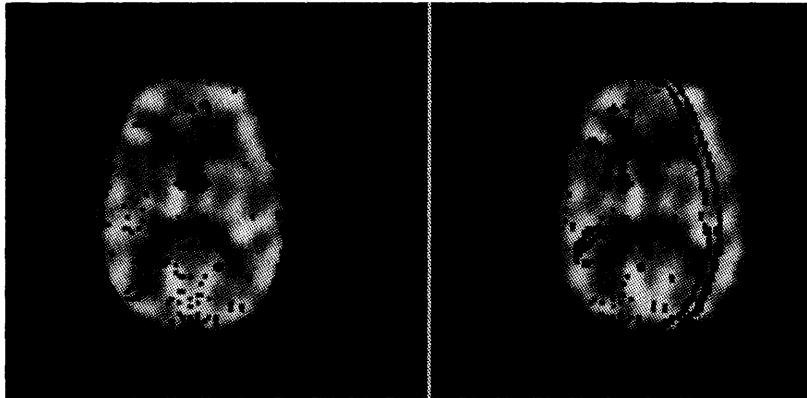
c)

Figure 4.4 Examples for the comparison window for registered and unregistered transverse brain images. a) mask, b) edges, c) fusion.

70

4.2.3 Registration of Thallium-201 studies

Registration using ALIGN is robust due to the abundance of information some of which is redundant. The redundancy of information is exhibited in the multiple ways by which the images are viewed. For example, for two images, front/back translation can be fixed using transverse planes and/or sagittal planes can be used, left/right translation can be fixed using transverse and/or coronal planes, and up/down translation can be fixed using coronal and/or sagittal planes. Although this redundancy is not intentional (i.e. three orthogonal views are necessary to fix the three angles of rotation), it is an important feature particularly when noisy images are encountered. An obvious example which can be registered successfully using ALIGN, while it is very difficult to register using the methods presented in chapter 3, is ^{201}Tl brain SPECT. Figure 4.5 shows an ALIGN page with ^{201}Tl-SPECT and MRI. In this case, registration is achieved by placing the boundaries of the brain on MRI in 3-D inside the cavity outlined by the ^{201}Tl-SPECT.
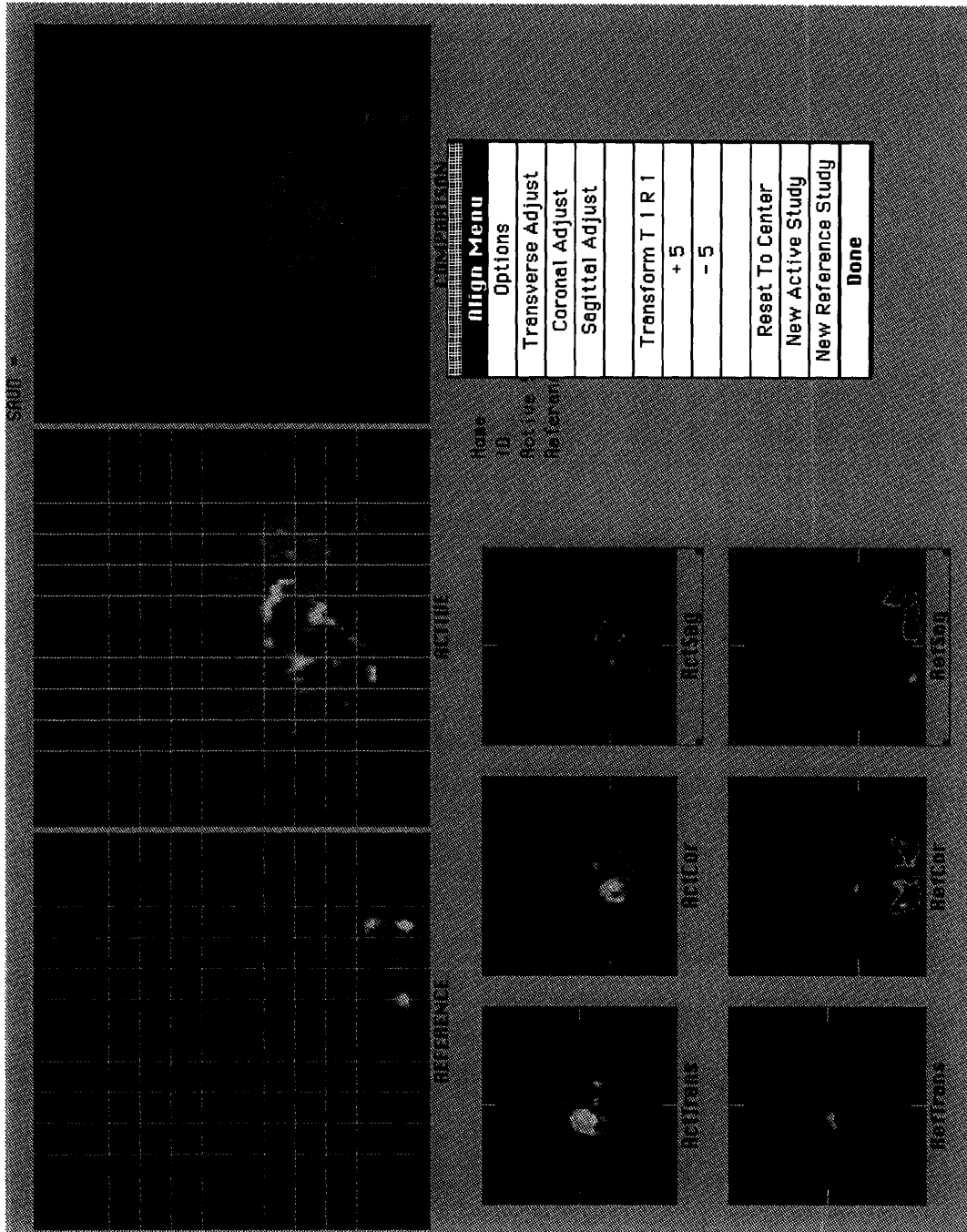
Figure 4.5 Thallium-201 brain SPECT and MRI registration.

4.3 Validation

In order to validate the accuracy of our method we performed two types of validation. The first type was performed using SPECTs and MRIs of a standard brain phantom (Hoffman brain phantom). The second type was performed using patient data. The goal was to assess the accuracy, consistency, and reliability of our method in SPECT/SPECT and SPECT/MRI registration and ascertain how it is affected by the amount of noise in the data.

4.3.1 Phantom Studies

Five SPECTs and one MRI scan were acquired using the Hoffman phantom. The SPECTs were performed using different amounts of ^{99m}Tc-prectechnetate yielding different count rates; Table 4.1 shows the total counts per study after reconstruction. The phantom orientation was not altered between SPECTs; thus, the five acquisitions were registered. SPECTs were reconstructed as described in section 4.1. SPECT 5 had the highest noise content, whereas SPECT 1 had the least. Typical brain SPECTs in the nuclear medicine department have counts in the range of 3-6 million after reconstruction. Therefore, SPECT 3 was selected as the reference to which the other SPECTs would be registered. The SPECTs were moved with random but known rotations and translations.

An MRI scan of the Hoffman phantom (filled with water) was obtained. The scan consisted of 49 slices (256 x 256) with a pixel size of 0.94x0.94 mm^2 and a slice thickness of 3.0 mm. The data

were transferred to the nuclear medicine department and processed as described in section 4.1.

Table 4.1   Counts in million for the five SPECT studies.

Study	SPECT 1	SPECT 2	SPECT 3	SPECT 4	SPECT 5
Counts	0.35	1.43	3.4	7.46	15.49

Two validation studies were performed using this data.   In the first validation, three individuals were asked to register the five displaced SPECTs to the reference SPECT which was not altered.   The resultant registration parameters were recorded and compared to the true orientations.   In this way, exact quantitative results about the quality of registration could be obtained.

In the second validation, the same individuals were asked to register the five SPECT studies to the MRI study.   The values of the transformations were recorded for all the operators.   Since the relative orientations of all the SPECTs with respect to each other were known, ideally, they should be transformed to the same location and orientation (same as the MRI) by the operators.   The differences in the targeted and the achieved transformations were compared to assess the accuracy of ALIGN.

4.3.2   Patient   studies

Eight pairs of clinical studies were recovered from the archives of the nuclear medicine department at Children's hospital (Boston, MA). These studies consisted of two MRI/MRI pairs, two perfusion SPECT/MRI pairs, two perfusion SPECT/perfusion SPECT pairs, and two ^{201}Tl-SPECT/MRI pairs. The same three operators, as in the previous section, were asked to register each of these pairs of studies. Since the exact orientation of these studies with respect to each others are not known, exact quantitative assessment of registration could not be obtained. Instead, the consistency among the three operators were analyzed as will be discussed in the results chapter.

Chapter 5

Results! Why, man, I have gotten a lot of results.
I know several thousand things that won't work.

— Thomas A. Edison

Results

Three points were used in the quantification of error. These points were selected on a 5.4 cm. radius to correspond to the centers of the top transverse, right sagittal, and front coronal slices of the brain, table 5.1. The final errors are the average of the errors in the registration of these points in pixels (1 pixel = 2.45 mm.).

Table 5.1   Test points coordinates in pixels.

	x	y	z
P 1	0	0	2 2
P 2	0	2 2	0
P 3	2 2	0	0

5.1   Phantom   registration

5.1.1 SPECT/SPECT

Table 5.1 shows the results of this study. With the exception of SPECT 1, the registration was accurate to within 1.5 pixels (3.6 mm.). SPECT 1 had the lowest counts and therefore the more noise of the

studies. This led to higher registration error (2.5 pixels, 6 mm.) (Figure 5.1).

Table 5.2 Results for SPECT to SPECT registration.

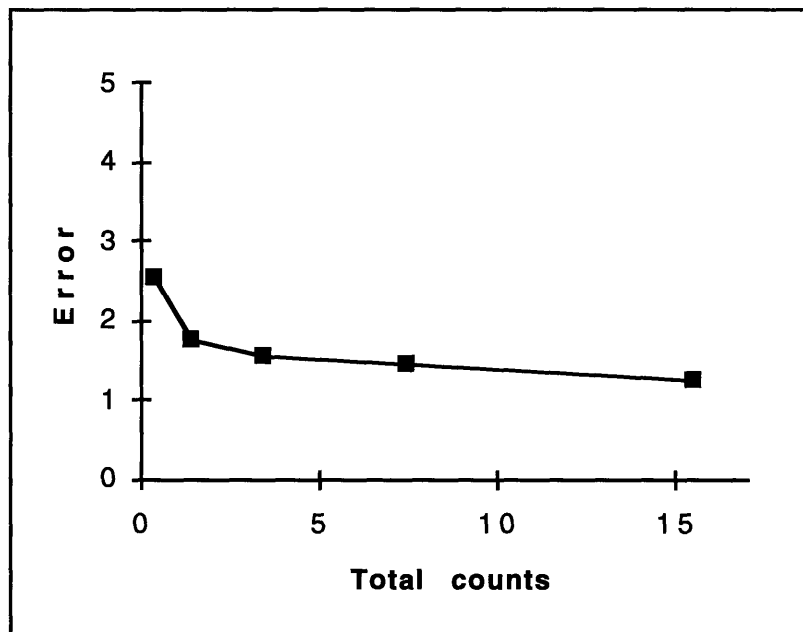|	Obs1	Obs2	Obs3	Obs1	Obs2	Obs3	Obs1	Obs2	Obs3	Avg
1	1.95	1.4	0.9	1.7	1.36	0.36	1.3	1.2	1	1.24
2	2	1.5	1.56	1.3	1.1	0.8	1.7	1.5	1.8	1.47
3	2	1.7	1.4	1.8	1.6	1.2	1.8	1.4	1.27	1.57
4	1.7	1.9	1.7	1.4	.99	.97	1.5	1.3	4.5	1.77
5	2.45	2.9	2.9	2.26	2.3	2.9	2.4	1.9	2.9	2.55

Figure 5.1 Average error in pixels vs. total number of counts in millions.

5.1.2 SPECT/MRI

The same three points described above were used to evaluate the error of registration. In this case, since the true location and orientation of the MRI with respect to the SPECTs is not known, exact quantification of the error is not possible. Instead, we compare the distance between the transformed points for the three operators. The operators aim at translating and orienting the active study to the reference study. Therefore, if registration using our program is reliable, the operators should translate and orient the active study with similar and consistent translation and rotation values. This consistency is described by the distance of the three test points. In other words, if the operators independently succeed to translate and rotate the active study with respect to the reference study with the same values, the distance between the points will be zero and therefore the error is zero. Conversely, if the operators orient the active study differently, then the error will be large. In this way, we are evaluating the consistency not the accuracy of registration among the operators.

Table 5.3 shows the results of this study. The values given are the average distance of the transformed three test points from the original points for each operator. Figure 5.2 shows the results in table 5.3 in a different way. The error for each operator is calculated as the difference between the average distances for the three test points from the average values of the three operators.

Table 5.3   Results for SPECT to MRI registration.

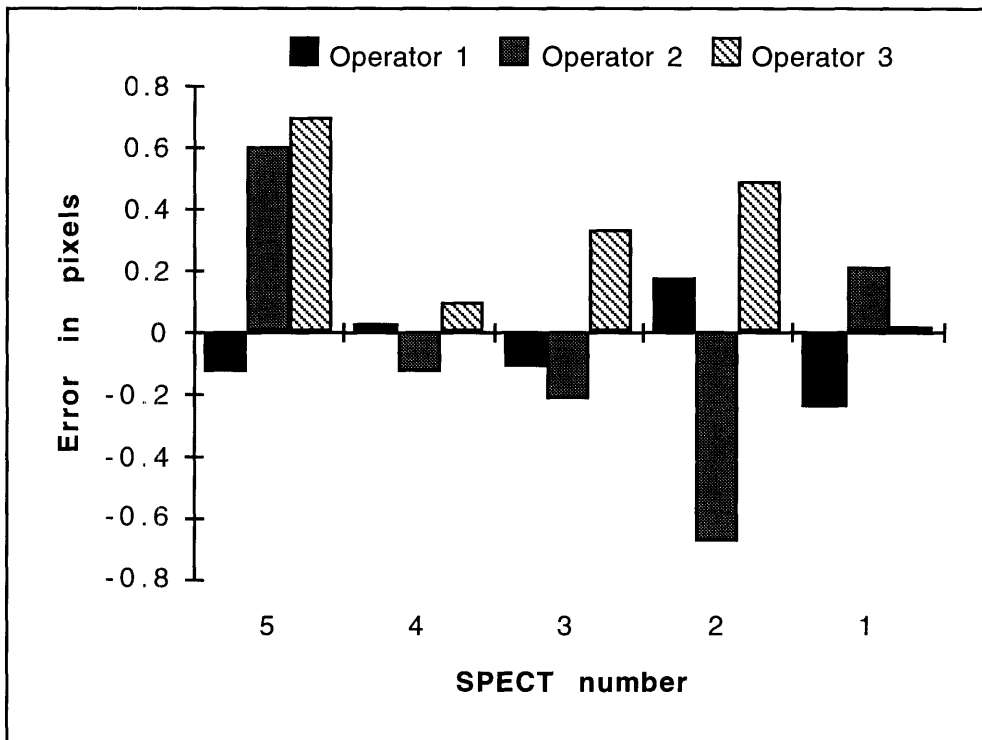|	Avg Op1	Avg Op2	Avg Op3	Avg
SPECT 1	1 3	14.7	15.1	14.4
SPECT 2	12.1	11.9	12.2	12.1
SPECT 3	2.8	2.7	3.3	2.9
SPECT 4	14.8	13.9	15.1	14.6
SPECT 5	5.2	5.6	5.5	5.4

Figure 5.2   Results for SPECT/MRI registration.

5.2 Patient registration

Registration of patient studies was evaluated in the same way as SPECT/MRI registration. Table 5.4 shows the results of this study. The values given are the average distance of the transformed three test points from the original points for each operator averaged over the two pairs for each category.. In figure 5.3, the error for each operator is calculated as the difference between the average distances for the three test points from the average values of the three operators.

Table 5.4 Average distance of the test points.

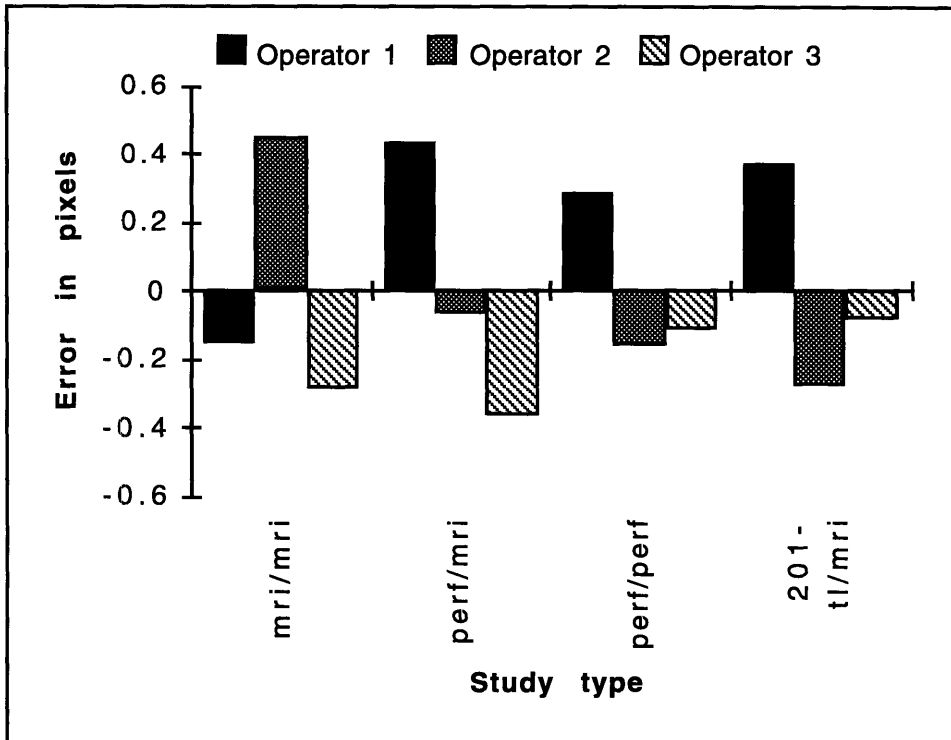|	Avg Op1	Avg Op2	Avg Op3	Avg
MRI/MRI	22.2	22.8	22.1	22.4
Perfusion/MRI	27.4	26.9	26.6	27
Perfusion/Perfusion	12	11.5	11.6	11.7
201Tl/MRI	17.7	17.1	17.3	17.4

Figure 5.3 Results for patient studies registration.

5.3 Discussion

The results of the validation studies show the strength of ALIGN. For SPECT-to-SPECT registration, with the exception of SPECT 5, the registration was accurate to within 1.8 pixels (4.4 mm.) (Figure 5.1). In the case of SPECT 5, total counts of 350 kcnts., internal structures and anatomy were not identifiable, and the operators relied on the external contours of the brain to guide the registration. This led to uncertainties in rotational registration, and the resultant error was higher than the rest of the cases (2.5 pixels, 6 mm.). The SPECT 1

example demonstrates the importance of internal structures in registration. Reliance on external contours is not sufficient to produce accurate registration. The same general remarks apply to the case of SPECT-to-MRI phantom registration and the patient studies in which the operators where independently consistent to within less that a pixels (< 2.45 mm.) of each others (Figures 5.2 and 5.3).

Chapter 6

'What is the use of a book' thought Alice 'without pictures'

-Alice's Adventures in Wonderland

Patient Studies

We have used ALIGN to register approximately 80 SPECT/SPECT and SPECT/MRI cases. These cases involved mostly brain images. The studies included (^{99m}Tc-HMPAO, ^{99m}Tc-ECD, ^{201}Tl, MRI/T1, MRI/T2, MRI/gadolinium). Registration was evaluated qualitatively by a trained observer.

The most common utility for ALIGN has been to register cases involving brain tumor and epilepsy. We have also used ALIGN to register activation studies. In the following sections, we will present some examples of these cases.

6.1 Tumor studies

The presence and viability of tumors can be assessed reliably using ^{201}Tl-SPECT. Viable tumors display higher trecer uptake than normal tissues, whereas necrosis and fibrosis show regions of lower uptake. Thus viable tumors look "brighter" than neighboring tissues on a perfusion study, whereas necrosis and fibrosis look "darker". ^{201}Tl has been shown to accumulate in active tumor tissues as

83

discussed in chapter 2. Since ^{201}Tl does not cross the blood-brain barrier, normal brain tissues appear dark on ^{201}Tl SPECTs while active tumor tissue appears bright. ^{201}Tl SPECTs contain very little anatomical details which make localization of the tumor tissues difficult to achieve. Therefore, cross registration of perfusion and ^{201}Tl SPECTs with anatomical modalities like CT and MRI is very desirable.

CT and MRI have high sensitivity and specificity in the diagnosis of brain tumors. However, these structural imaging modalities are limited in their ability to assess tumor viability. They are often unable to differentiate between tumor presence and nonspecific brain injuries. Also, it is generally difficult to distinguish between tumor tissue and necrosis or fibrosis and to define the extent of the tumor (Treves 95).

In the following sections, we will show some examples of brain tumor images. We will demonstrate the importance of cross registration in the diagnosis and localization of viable tumors.

Case 1. Tl-201 SPECT and MRI

This is a 10 year old female with a brain tumor (Figure 6.1). ^{201}Tl SPECT shows a focal area of increased uptake in the posterior fossa. The size of the abnormality is smaller than that seen on MRI. This suggests that part of the abnormality seen on MRI is due to tumor necrosis or fibrosis rather than the viable tumor itself.

Case 2. Tl-201 SPECT and MRI

This is a 15 year old female with persistent headache. It was found that she had a brain tumor (Figure 6.2). ^{201}Tl brain SPECT shows a large area of thallium uptake in the right temporal-parietal region. This is indicative of a viable tumor. The location of the viable tumor corresponds to the abnormality seen on MRI. However, the area of active tumor is smaller on ^{201}Tl-SPECT than on MRI.

Case 3. HMPAO-SPECT and Tl-201 SPECT

This a 5 year old male with a brain tumor (Figure 6.3). Two studies are shown, a perfusion study, ^{99m}Tc-HMPAO-SPECT, and a ^{201}Tl-SPECT. There is evidence of thallium-avid residual tumor following radioactive therapy in the midline posterior fossa. Surrounding the increased thallium uptake is a zone of reduced perfusion. No overlay of images is shown.
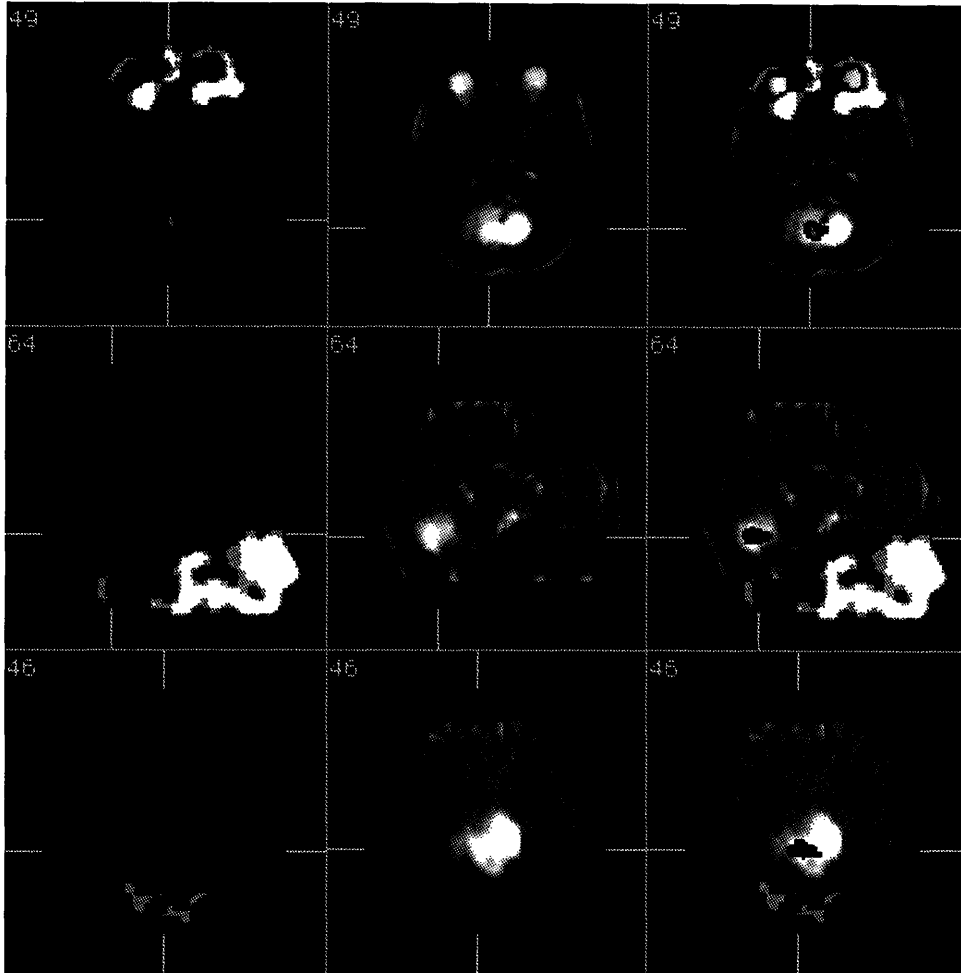
Figure 6.1 Brain tumor shown on 201Tl-SPECT (left), MRI (center), and a fusion image (right).
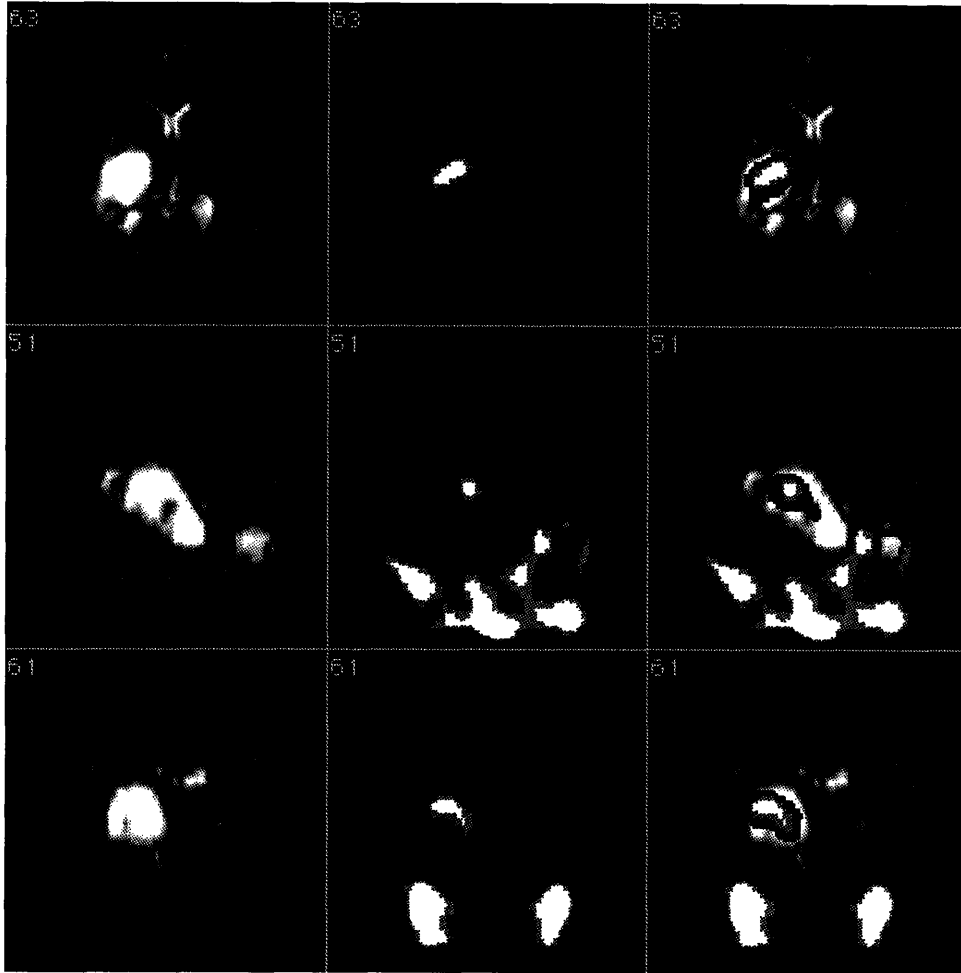
Figure 6.2 Brain tumor shown on MRI (left), ^{201}Tl-SPECT (center), and a fusion image (right).
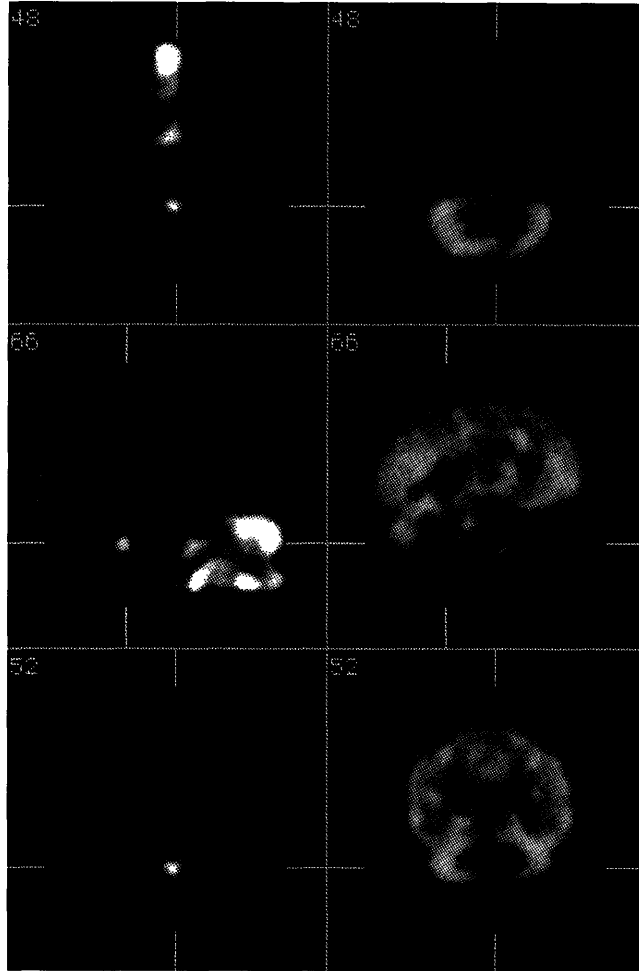
Figure 6.3 Posterior fossa tumor shown on ^{201}Tl-SPECT (left), and ^{99m}Tc-HMPAO-SPECT (right). On the left image, bright corresponds to high ^{201}Tl uptake, while dark corresponds to low or no uptake. On the right image, bright corresponds to high perfusion, while dark corresponds to low perfusion.

6.2 Epilepsy studies

Epilepsy is usually controlled with considerable success with medications. Some patients, however, do not respond to medical therapy. This called medically refractory epilepsy. Surgical removal or disconnection of the portion of the brain that contains the epileptogenic focus has been found to control seizures in many patients with medically refractory epilepsy (Treves 95). When surgery is deemed necessary, accurate localization of the epileptogenic focus is crucial. It would be disastrous to operate on the wrong site or to overlook a second active site. Consequently, a battery of tests using electroencephalograph (EEG), SPECT, and in some cases PET is employed to verify localization. Since none of these modalities provide accurate anatomical localization, cross registration with CT and MRI is desirable.

Perfusion brain SPECT in patients with epilepsy have revealed characteristic time dependent changes in regional cerebral perfusion. Generally, on ictal SPECT, increased perfusion is observed at the site of the epileptogenic focus. This is followed during the interictal period by hypoperfusion in the same and surrounding regions. These perfusion abnormalities are frequently accompanied by normal or almost normal CT or MRI scans.

SPECT while having a high functional resolution, is an inherently noisy. Consequently, small changes of perfusion during epilepsy may be hard to detect on single scans. A second scan, base line scan, is

usually employed to compare regional perfusion defects. In the case of epilepsy, an ictal scan, during seizure, and an inter-ictal scan, during a seizure free time, are used to improve the localization of epileptogenic foci. These ictal and interictal SPECTs should be registered accurately so that corresponding regions can be compared to emphasize perfusion changes.

In the following sections, we present typical registered images of selected patients with epilepsy:

Case 1. 99m-Technetium-HMPAO-SPECTs

This is a 7 year old female with intractable partial epilepsy (Figure 6.4). The ictal study shows increased focal perfusion in the right posterior frontal/temporal cortex corresponding to a region of hypoperfusion in the inter-ictal study. This suggests an epileptogenic focus in this area.

Case 2. 99m-Technetium HMPAO-SPECTs

This is a 12 year old female with intractable epilepsy (Figure 6.5). Inter-ictal SPECT shows markedly abnormal perfusion with multifocal areas of reduced cerebral blood flow. Ictal SPECT shows a small area of focally increased perfusion in the right prefrontal area as well as in the left posterior thalamus.

Case 3. 99m-Technetium HMPAO-SPECTs and MRI

This is a 8 year old male with complex partial seizures (Figure 6.6). Inter-ictal study shows no perfusion abnormalities. MRI study

shows no structural abnormalities. Ictal SPECT shows an intense focal hyperpefusion in the left posterior frontal cortex.
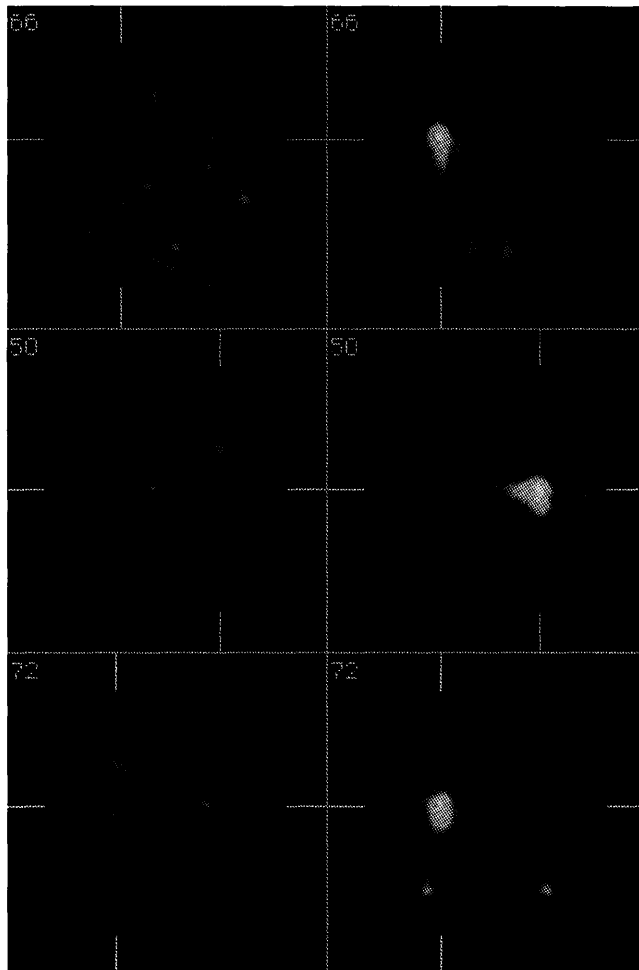
Figure 6.4 Increased perfusion on ictal (right) and hypoperfusion on inter-ictal (left). Yellow corresponds to high perfusion while blue to low perfusion.
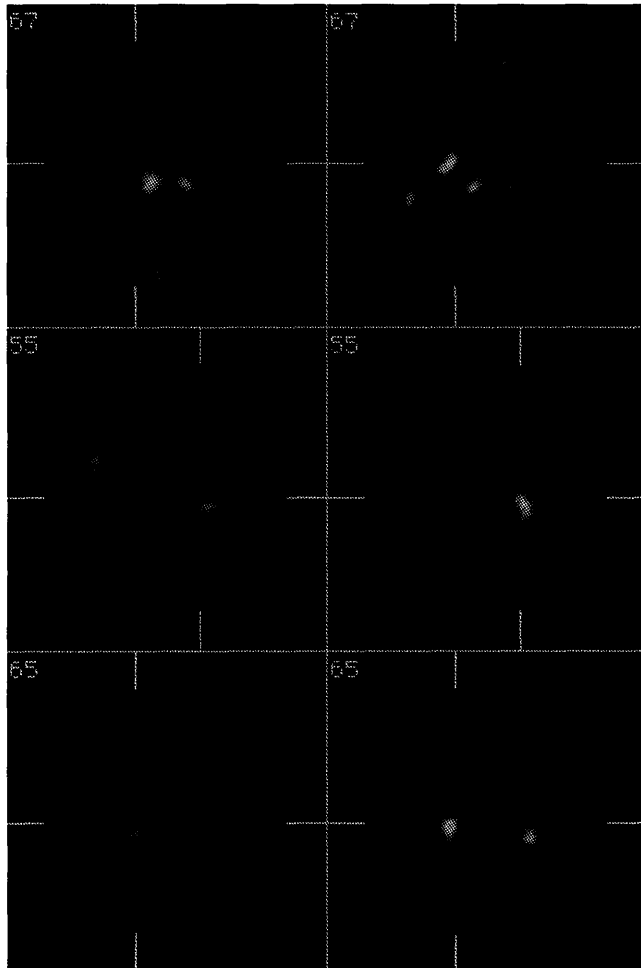
Figure 6.5 Multifocal defects on inter-ictal (left) with focally increased perfusion on ictal (right). Yellow corresponds to high perfusion while blue to low perfusion.
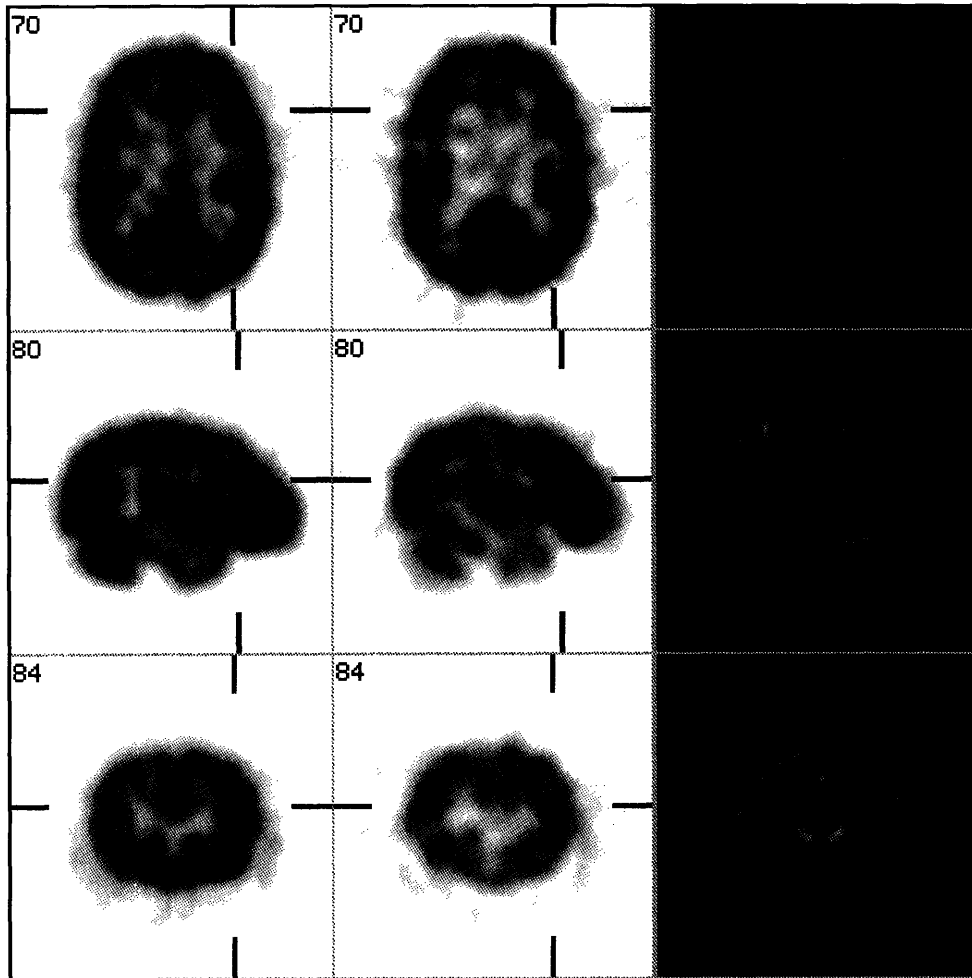
Figure 6.6 Complex partial seizures with normal inter-ictal SPECT
(left) and MRI (right) and abnormal ictal SPECT (center). Yellow
corresponds to low perfusion while black to high perfusion.

6.3 Activation studies

Activation studies involve two perfusion brain SPECTs during two different states of brain activation. The first study is called the baseline scan. During injection, care is taken to reduce as much as possible patient anxiety, sensory stimulation, and motor activity. For the activation study, the patient is instructed to perform a specific task for few minutes and the tracer is given during the task. The task may involve repetitive visual, auditory, or somatosensory stimulation (Treves 95).

Figure 6.7 shows an example of an activation study. This is a 10 year old female with speech defects and learning problems. A baseline brain SPECT was acquired with injection of ^{99m}Tc-HMPAO while the patient was instructed to read words. The words were written in different colors. The patient was instructed to only read the words ignoring the colors.

Following the baseline study, the Stroop test, which is a cognitive activation procedure, was administered. During the test, the patient was injected with the tracer. Few minutes later, another SPECT was obtained.

In the baseline study, there is a marked increase in tracer distribution to the left temporal cortex and a prominent activation of the visual cortex. This is consistent with activation by reading task.

In the second study, a slight reversal of perfusion is noted in the supratentorial structures. Also, the visual cortex is less prominently activated than in the baseline study. This is consistent with the Stroop test which is believed to involve cortical inhibition.
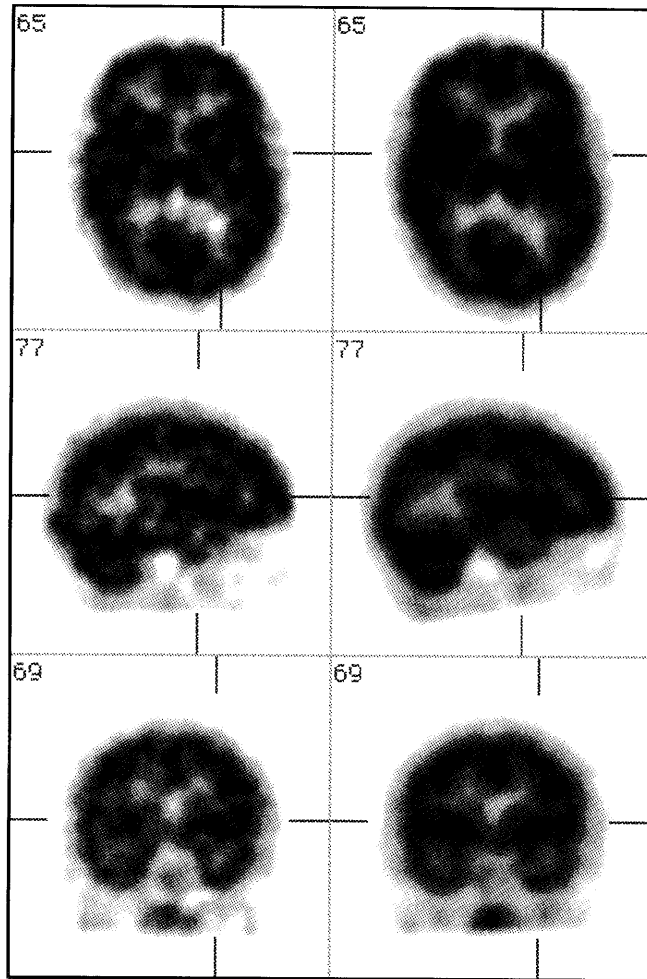
Figure 6.7 Example of an activation study. Baseline on left and activation on right. Black correspond to high perfusion while white to low perfusion.

Chapter 7

*Not only to say the right thing in the right place,
but far more difficult, to leave unsaid the wrong
thing at the tempting moment.*

— George Sala

*Drawing on my fine command of language, I said
nothing.*

— Robert Benchley

Conclusion

Frequently, in automated image registration, the mathematical
models used to represent the data are inaccurate or insufficient. In
such cases, the registration algorithm fails to achieve the desired
result, and a different approach has to be selected. Although some
algorithms have been shown to work reasonably well in some cases
it is an extremely difficult task to design an algorithm that will work
predictably for all imaging modalities. Furthermore, no single
criterion has been shown to give an accurate quantitative assessment
of registration. In any case, the final decision on the validity of any
registration is left to a trained operator. We have based the design
of ALIGN on this premise. ALIGN provides the operator with all the
available information about the images in a clear and concise way. It
also provides the operator with easy and intuitive tools to
manipulate the orientation and position of the images. The decision
on translations or rotations is left to the operator. After any change,

real time feedback shows the most recent location and orientation of the images in 3-D. This serves to guide the operator through registration. The result is an easy-to-use, simple, and accurate general purpose registration algorithm.

The robustness of ALIGN has been demonstrated clearly in a number of case. First, with the exception of the very noisy images, registration of perfusion SPECT/SPECT studies is achievable with errors less than 1.8 pixels (see section 5.3). Second, ^{201}Tl-SPECT registration with MRI or perfusion SPECT is attainable with acceptable errors as evaluated and inspected by a group of trained operators. This is a unique feature of ALIGN which is not directly achievable using the other registration approaches described in chapter 3.

A very important and unique feature of our method is the ability to align single studies (see section 4.2). Usually, head alignment is done at the beginning of the scan by the careful positioning of the patient in the gantry. However, occasionally SPECTs need to be reoriented so that symmetric regions of the brain can be appropriately compared. This can be done easily and reliably using ALIGN. Conversely, this feature is not considered in the design of other registration methods (Chapter 3).

In conclusion, we have presented a new algorithm for the alignment and registration of 3-D medical images acquired using SPECT and MRI. We have described the algorithm and presented arguments

and results to demonstrate its robustness. However, ALIGN is not presented as the ultimate solution to medical image registration. The correct choice of a specific method of registration is task dependent. The final choice on what method and algorithm to use is best made by the operators and the ultimate quality of fit and robustness of registration is left to the trained eye. As of our experience with SPECT and MRI at the nuclear medicine department at Children's hospital (Boston, MA), ALIGN has performed exceedingly well.

References

[1] Venot A, Lebruchec JF, Roucayrol JC. A New Class of Similarity Measures for Robust image registration. *Comput Vis Graph Image Process,* 1984;28:176-184.

[2] Venot A, Liehn JC, Lebruchec JF, Roucayrol JC. Automated comparison of scintigraphic images. *J Nucl Med* 27:1337-1342, 1986.

[3] Svedlow M, McGillem C, Anuta P. Image registration: similarity measure and preprocessing method comparisons. *IEEE Trans Aerospace and Elec Sys,* 1978; vol. AES-14 no 1:141-149.

[4] Treves, S. T. Pediatric nuclear medicine, 2nd ed. Springer-Verlag New York Inc., 1995.

[5] Jaszczak, R. J. Tomographic Radiopharmaceutical Imaging. *Proc IEEE,* vol. 76, no. 9, Sept. 1988.

[6] Sorenson, J. A. Physics in nuclear medicine, 2nd ed. Grune & Stratton, Inc., 1987.

[7] Brooks, R. A., Di Chiro, G. Principles of Computer Assisted Tomography (CAT) in Radiographic and Radioisotopic Imaging. *Phys Med Biol* , Vol. 21, No. 5, 689-732, 1976.

[8] Anger, H. O. A new instrument for mapping gamma ray emitters. *Biology and Medicine Quarterly Report* , UCRL-3653, p. 38, Jan 1957.

[9] Chen, Q. S. Image Registration and Its Application in Medical Imaging. *PhD thesis, Vrije Universiteit Brussel,* Dec 1993.

[10] Corria, J. A. Editorial: Registration of Nuclear Medicine Images. *J Nuc Med,* 1990;31:1227-1229.

[11] Erickson, B. J., Jack C. R. Correlation of Single Photon Emission CT with MR Image Data Using Fiduciary Markers. *AJNR* May/Jun 1993,14:713-720.

[12] Loats, H. CT and SPECT Image Registration and Fusion for Spatial Localization of Metastatic Processes Using Radiolabeled Monoclonals. *J Nucl Med* , March 1993, Vol. 34, No. 3.

[13] Shukla, S. S., Honeyman, J. C., Crosson, B., Williams, C. M., Nadeau, S. E. Method for registrering Brain SPECT and MR Images. *J Comput. Assis. Tomogr* , 1992; 16(6):966-970.

[14] Pelizzari CA, Chen GTY, Spelbring DR, Weichselbaum RR, Chen C-T. Accurate three-dimensional registration of CT, PET, and/or MR images of the brain. *J Comput Assist Tomogr,* 1989;13:20-26.

[15] Siddon, R. L. Prism representation: a 3D ray-tracing algorithm for radiotherapy applications. *Phys Med Biol* ,30:817-14, 1985.

[16] Barrow HG, Tenenbaum JM, Bolles RC, et al. Parametric Correspondence and Chamfer Matching: Two New Techniques for Image Matching. *Proceed 5th Int Joint Conf Artificial Intelligence,* Cambridge, MA, 1977;659-663.

[17] Borgefors G. Distance transformation in arbitrary dimensions. *Comput. Vision, Graphics, Image Processing*, vol. 27, pp. 321-345, 1984

[18] Jiang H., Holton, K., and Robb, R. Image regisration of multimodality 3-D medical Images by chamfer matching. *SPIE Vision & Visualization Conference in San Jose, CA*, Feb 9-14, 1992.

[19] Alpert NM, Bradshaw JF, Kennedy D, Correia JA. The principal axes transformation: a method for image registration. *J Nuc Med,* 1990;31:1717-1722.

[20] Rusinek, H., Tsui, W., Levy, A. V., Noz, M. E., de Leon, M. J. Principal Axes and Surface Fitting Methods for Three-Dimensional Image Registration. *J Nucl Med* 34:2019-2024, 1993.

[21] Junck, L. Moen, J. G., Hutchins, G. D., Brown, M. B., Kuhl, D. E. Correlation Methods for the Centering, Rotation, and Alignment of Functional Brain Images. *J Nucl Med* 31:1220-1276, 1990.

[22] Bacharach, S. L., Douglas, M. A. Carson, R. E. et. al. Three-Dimensional Registration of Cardiac Positron Emission Tomography Attentuation Scans. *J Nucl Med* 34:311-321, 1993.

[23] Minoshima, S., Berger, K. L., Lee, K. S., Mintum, M. A. An Automated Method for Rotational Correction and Centering of Three-Dimensional Functional Brain Images. *J nucl Med* 33:1579-1585 1992.

[24] Hoh, C. K., Dahlbom, M., Harris, G. et.al. Automated Iterative Three-Dimensional Registration of Positron Emission Tomography Images. *J Nucl Med* 34:2009-2018, 1993.

[25] Woods PP, Cherry SR, Mazziotta JC. Rapid Automated Algorithm for Aligning and Reslicing PET Images. *J Comput Assist Tomogr,* 1992;16(4):620-633.

[26] Woods PP, Mazziotta JC, Cherry SR. MRI-PET Registration with Automated Algorithm. *J Comput Assist Tomogr,* 1993;17(4):536-546.